



Characteristics of atmospheric boundary layer structure using monostatic SODAR system over Mumbai region

NISHANT KUMAR^{1,2}, ANJALI S NAIR³, KIRTI SONI^{1,*}, A A SHINGARE⁴,
VIDYANAND M MOTGHARE⁴, KARANSINGH A RAJPUT⁴, V K SONI⁵,
ANIKENDER KUMAR⁵ and ARVIND KUMAR JHA⁶

¹CSIR-Advanced Materials and Processes Research Institute (AMPRI), Bhopal 462 026, India.

²Koneru Lakshmaiah Education Foundation (KLEF), Guntur 522 302, India.

³CSIR-National Physical Laboratory (NPL), Dr. K. S. Krishnan Marg, New Delhi 110 012, India.

⁴Maharashtra Pollution Control Board, Mumbai 400 022, India.

⁵India Meteorological Department, Lodi Road, New Delhi 110 003, India.

⁶Central Pollution Control Board, Regional Directorate, Vadodara, Gujarat, India.

*Corresponding author. e-mail: 2006.kirti@gmail.com

MS received 12 May 2022; revised 11 July 2023; accepted 23 July 2023

Atmospheric Boundary Layer (ABL) height variability, along with meteorological parameters and pollutant concentrations, are studied during different months in Mumbai region for the period of November 2020 to October 2021. ABL height is measured using a monostatic SODAR (SOmic Detection And Ranging) system. The capabilities, behaviour, and benefits of employing this ground-based remote sensing system in Mumbai are examined in this preliminary report after a year of SODAR monitoring. SODAR dataset is also compared with Radiosonde input ERA5 reanalysis data. The ventilation coefficient (VC) analysis for the same time period is also covered in the paper. Especially in the months of November, December, January, February, August, September, and October, the ABL height often approached 700 m. The ABL height is increased to 1000–1200 m in April because of the strong winds and warm weather. The month of April has the greatest monthly average height (418 m), while the month of February has the lowest monthly average height (179 m). In April, when the wind speed is 7.2 m/s, the convection duration is observed to be the longest, while in December, when the wind speed is 1.75 m/s, it is the shortest.

Keywords. Atmospheric boundary layer; SODAR; ventilation coefficient; air pollution; dispersion; air quality.

1. Introduction

The troposphere is the atmosphere's lowest layer. Weather, cyclones, and anticyclones are all part of it. It stretches from the earth's surface to a height of roughly 15 km, with the upper limit fluctuating

depending on the site's geographical position (i.e., from pole to equator) (Stull 1988). Its permanent constituents are nitrogen, oxygen, argon, and carbon dioxide, with their relative concentrations essentially unaltered (Kumar *et al.* 2021a). In addition, the troposphere contains several

additional changeable elements, the most prominent of which are ozone and water vapour. Near the earth's surface, the largest concentration of water vapour can also be observed. Wind speed is also shown to rise with height, but pressure falls consistently with height, temperature decreases less consistently, and humidity decreases quite erratically (Stull 1988). The atmospheric boundary layer (ABL) is the lowest portion of the troposphere where the direct effect of surface heating and cooling can be seen (Kumar *et al.* 2021a). All biological and human activities take place within this layer. The ABL extends to the height of convective mixing of buoyant parcels of air or the base of an elevated inversion layer under conditions of strong upward heat flux, i.e., under daytime unstable conditions, and the level of surface-based inversions determines the height of the ABL during night-time, i.e., under stable conditions (Kumar *et al.* 2017a). Turbulence is one of the ABL's most important components. It allows transporting water vapour, heat, momentum, contaminants, and other tracer components from one location to another.

Many factors control the air quality at a place at any time of the day (Garratt 1994). Some of these factors are constant for a particular location, while others are variable. The constant ones include the topography and climatology of the place, nature of the pollution sources in and around that place, nature and amount of the effluent and the demography of that location (Bontempi and Coccia 2021). The variable factors are the time distribution of emission, synoptic weather pattern, meso-scale low-level stability, inversion topography and depth, and flow pattern. Careful examination of meteorological parameters reveals that only two factors can be classified as key in managing pollution concentrations in a specific area with a set of constant controls. These are the low-level temperature structure and low-level wind direction and strength (Stull 1988). The low-level temperature structure determines whether the atmosphere is in a state of static stability or instability and under these conditions, diffusion of pollutants is either suppressed or enhanced (Liao *et al.* 2021). The wind velocity, on the other hand, determines the path the pollutants will take after the emission and how rapidly the effluents will be carried away. These conditions are thus a necessary input to determine whether a given emission rate will produce a critical concentration level over a region.

In light of the importance of the atmospheric structure and dynamic processes in the lower atmosphere to a wide range of human endeavours, various types of monitoring techniques have been developed over time to monitor the atmospheric parameters such as temperature, humidity, wind speed and direction, and their distribution in space (Stull 1988). *In-situ* procedures and remote sensing techniques are the two primary categories for these methods. The details of these techniques are mentioned by Seibert *et al.* (2000).

SODAR (SONic Detection And Ranging) is a device based on remote sensing to monitor the ABL and their structure (Kumar *et al.* 2014, 2021b, c). SODAR has the best refractive index among other remote sensing instruments. It is internationally recognised and recommended by the Environmental Protection Agency (EPA) for air quality modelling in the Environmental Impact (EIA) Assessment (Stull 1988, EPA Report 2000). SODAR is the cost-effective instrument for real-time monitoring of ABL heights up to 1–2 km. The Bhopal Gas Tragedy attracts the scientific community to study ABL to measure the VC of an area. Given the conditions, the Central Pollution Control Board (CPCB) Delhi has been included SODAR system in the list of mandatory equipment for air quality management to avoid such disasters (CPCB Report 1992).

SODAR is one of the best remote sensing systems recognised worldwide and has proven effective in providing real-time data on air pollution controls such as mixing height (ABL height)/altitude conversion. This is the first time that the SODAR system has been installed in Mumbai region (near the coastal region, Sion). It is the first time that such an analysis using ABL height real-time hourly data is being performed over Mumbai region. SODAR provides useful information for the investigation of parameters relevant to air pollution studies. In the present paper, different structures of ABL height along with ventilation coefficient have been studied, and ABL height comparison with meteorological parameters also discussed.

2. Geographical study of the Mumbai region and monostatic SODAR details

Increasing air pollution in Mumbai city is one of the significant problems for policymakers. The geography of Mumbai results in the advection of

air into the city from the surrounding areas, which can sometimes be significantly more polluted than the city centre itself (Kumar *et al.* 2016). Mumbai is on a narrow peninsula on the southwest of Salsette Island, which lies between the Arabian Sea to the west, Thane Creek to the east and Vasai Creek to the north (figure 1).

2.1 Details of MPCB SODAR system

MPCB has deployed a monostatic SODAR at Mumbai that provides information on the thermal structure of the lower atmosphere. The installation of the SODAR at the MPCB headquarters is completed in November 2020. The study location is at the intersection of 72.865°E longitude and 19.042°N latitude. As per the topography, the area is located far away from the sea is ~3 km. The atmospheric turbulent eddy diameters that cause acoustic wave scattering are on the order of half a wavelength. The SODAR provides information about thermal plumes, inversion layer breaking periods, boundary layer heights, mixing layers, and other related phenomena in time and space.

Based on the foregoing considerations, the backscattering monostatic SODAR system is designed and developed (Aggarwal *et al.* 1980; Singal *et al.* 1985; Gera *et al.* 2011; Kumar *et al.* 2021a, b). Figure 2 shows a schematic block diagram for the monostatic SODAR. It is used in a monostatic mode antenna emitting high power acoustic burst of 100 ms duration every six

seconds at acoustic centred frequency 2250 Hz (Kallistratova 1963; Brown and Hall 1978). The technique is used by transmitting a pulsed narrow sound beam into the atmosphere, where air inhomogeneity is contacted and partially reflected. It has received dispensed signals from the same transducer. With each echo scan, the time of delay and intensity are measured as intensity module on the PC, with visually displayed in either operational mode the height range (ordinate) *vs.* the time (abscissa). The two main kinds of acoustic echoes seen in echograms are inversion echoes and thermal echoes. Thermal echoes appeared as vertical intermitted spikes, whereas inversion echoes were horizontal and continuous in time. An acoustic wave propagating through a turbulent medium gets scattered, refracted, and attenuated. The basic data is acquired by using the monostatic SODAR system. The operation parameters are shown in table 1.

In the new SODAR system, an Ultra-Low-Noise Amplifier (ULNA) and Dual-Amplifier Band Pass (DABP) filter are designed for analog signal conditioning of SODAR (Chourey *et al.* 2022a, b). The updated analog signal conditioning system features improved gain and high signal-to-noise ratio (SNR) of 65 and 92 dB, respectively. The results were then compared with the existing analog signal conditioning system. It was observed that the updated system has significant advantages in terms of gain and narrow bandpass response. Additionally, the updated SODAR system captured the echogram structures. The results demonstrate the efficiency

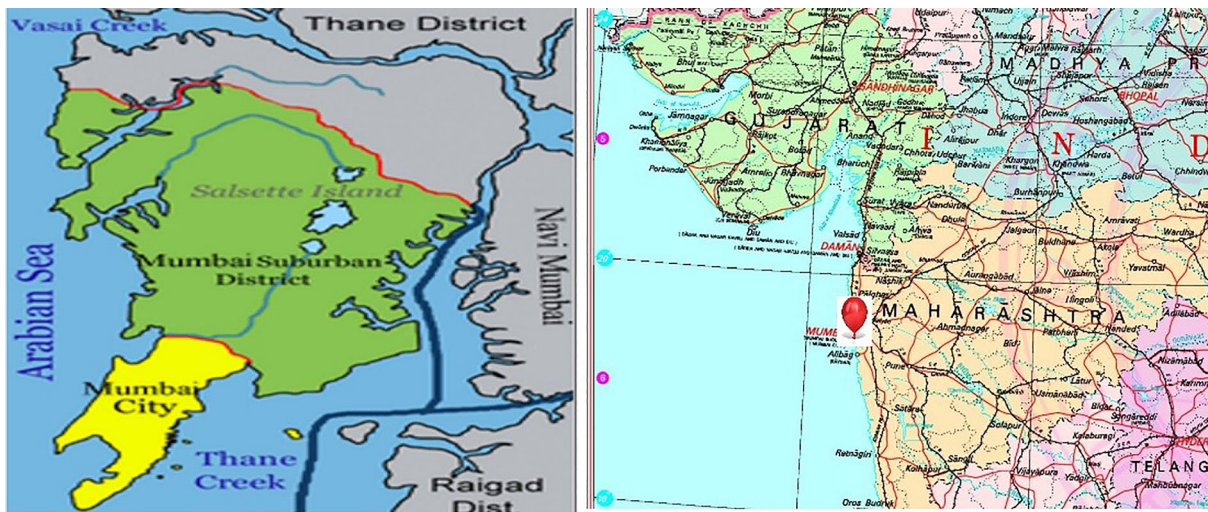


Figure 1. Map of Mumbai City (courtesy: www.mapindia.com).

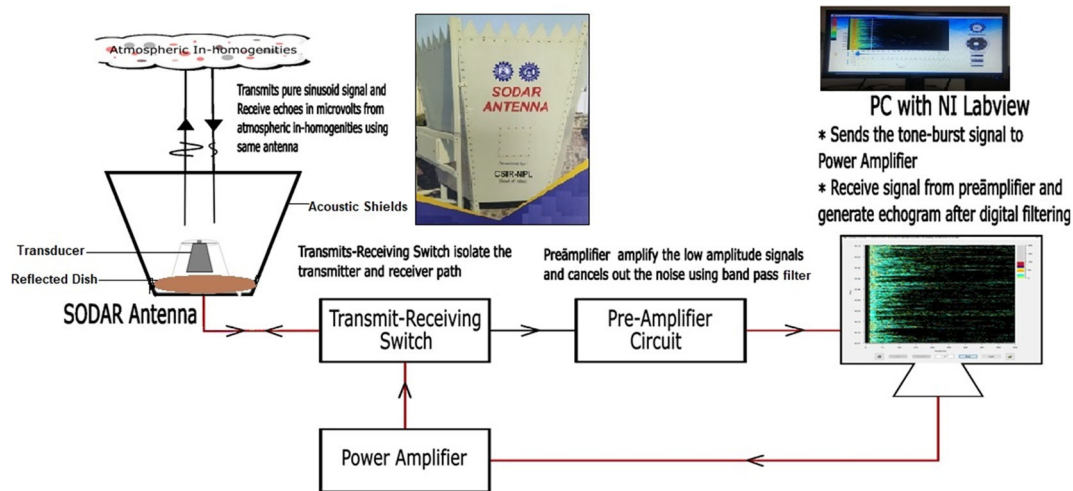


Figure 2. Block diagram of SODAR system.

Table 1. Specifications of monostatic SODAR system.

Transmitted power (electrical)	90 Watts
Transmitted power (acoustical)	15 Watts
Pulse width	100 ms
Pulse repetition period	6 sec
Operational range	1000 m
Receiver bandwidth	100 Hz
Frequency of operation	2250 Hz
Acoustic velocity	340 m/s (average)
Receiver gain	66 dB
Transmit-receive antenna	Parabolic reflector dish
Receiver area	2.5 m ²
Preamplifier sensitivity	60 μ V (theoretical calculation)

of the echogram in capturing the well-known standard structures of ABL.

A unique software is developed for monitoring and storing all the data observed by SODAR on a LABVIEW platform (online software and offline software) (Kumar *et al.* 2021b, c). The system consists of two software. (1) Online Software, which is responsible for running the SODAR system, acquiring and logging FAX plots as well as weather data. (2) Offline Software, wherein the user can view historical SODAR data, do detailed studies as well generate reports.

This new updated version of the SODAR system has a set of meteorological sensors integrated into it, thus providing valuable insight into temperature, humidity, wind speed and wind direction data, which can be related to the ABL height

variations in the lower atmosphere. The system is capable of monitoring the ABL up to a height of 1000 m. The observation period from 5th November 2020 to 31st October 2021 is used in this study.

2.2 ABL height determination from SODAR echogram

The SODAR is a cost-effective remote sensing system that uses sound waves. It allows 24 \times 7 monitoring. A SODAR emits sound pulses at various heights of the atmosphere and receives back dispersed pulses in temperature inhomogeneities. SODAR echograms provide lower climate turbulence pictures as well as contaminant distribution responsibilities. Based on the vertical profile of the acoustic refractive index shown in figure 3, the echogram (9th May 2021), atmospheric conditions are divided into two categories: convective period (unstable) and non-convective (stable) period (output of SODAR). Beyrich (1997), Singal *et al.* (1997) and Bradley (2007) have compiled methods and algorithms for calculating the ABL height using SODAR data. Being based on sonic principles, the range of SODARs is limited to a few hundred meters, extending a maximum of up to 1000 m based on the power and frequency of the emitted pulse. The observer needs to broadly classify the data into two categories, namely: inversion-time and convection-time. The other classifications of ABL structure are fog-layer, rising-layer, multi-layer, *etc.*, and each classified structure demands a different approach for the ABL height estimation. The structures are manifestations of different prevailing meteorological

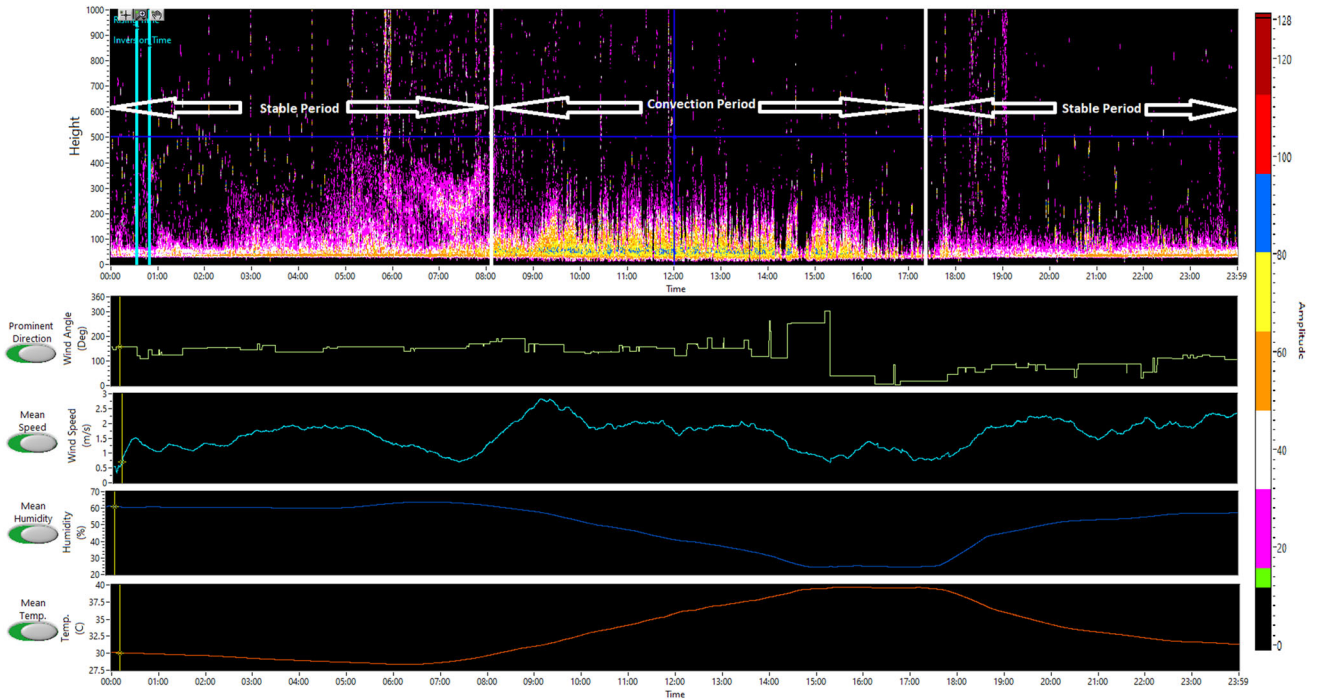


Figure 3. Stable and convective period on SODAR Echogram (9th May 2021).

conditions. The meteorological processes responsible for generating such structural SODAR signatures include phenomena such as free/forced convection, nocturnal cooling of ground, sea breeze, land breeze, advection, subsidence, frontal system, etc. These phenomena generate a turbulence zone boundary in ABL, which in turn acts as a tracer for SODAR interrogation.

The ABL height has been directly picked up from the echogram by using visualisation, apart from the convection period. A measurement of the height of the thermal plumes by SODAR during the day will always give an underestimated value unless they are capped by a low-level elevated shear echo layer; however, as SODAR sensitivity declines in the daytime compared to the nighttime due to the prevalent ambient noise which decreases its probing range. Based on a Holzworth model and radiosonde data for Delhi, a method to estimate mixing height during the daytime when the plumes are not covered by a stable layer has been developed (Singal 1993; Singal *et al.* 1994). Therefore, the actual ABL height is determined by using an empirical formula equation (1) (Singal *et al.* 1985).

$$y = 4.24x + 95, \tag{1}$$

where y is the calculated ABL height and x is the observed thermal plume height in the echogram. This formula was determined by comparing SODAR data with Radiosonde data (Singal and Aggarwal 1979).

3. Results and discussion

3.1 Sea breeze and their signature on SODAR echogram

Sea breeze is a phenomenon occurring in the coastal region and is associated with the manifestation of onshore local winds which set in from the sea onto land in the late forenoon or early afternoon. The phenomenon is marked by drop in surface temperature, rise in humidity level, change in wind direction, increase in wind speed and suppression of convective activity. Temperature differences between land and water surfaces give rise to the circulation of land and sea breeze. Sea breeze is especially well developed on a clear sunny day under conditions of calm to light winds. The land–sea temperature contrast is usually reversed at night, resulting in land breeze, which is weaker than the daytime sea breeze.

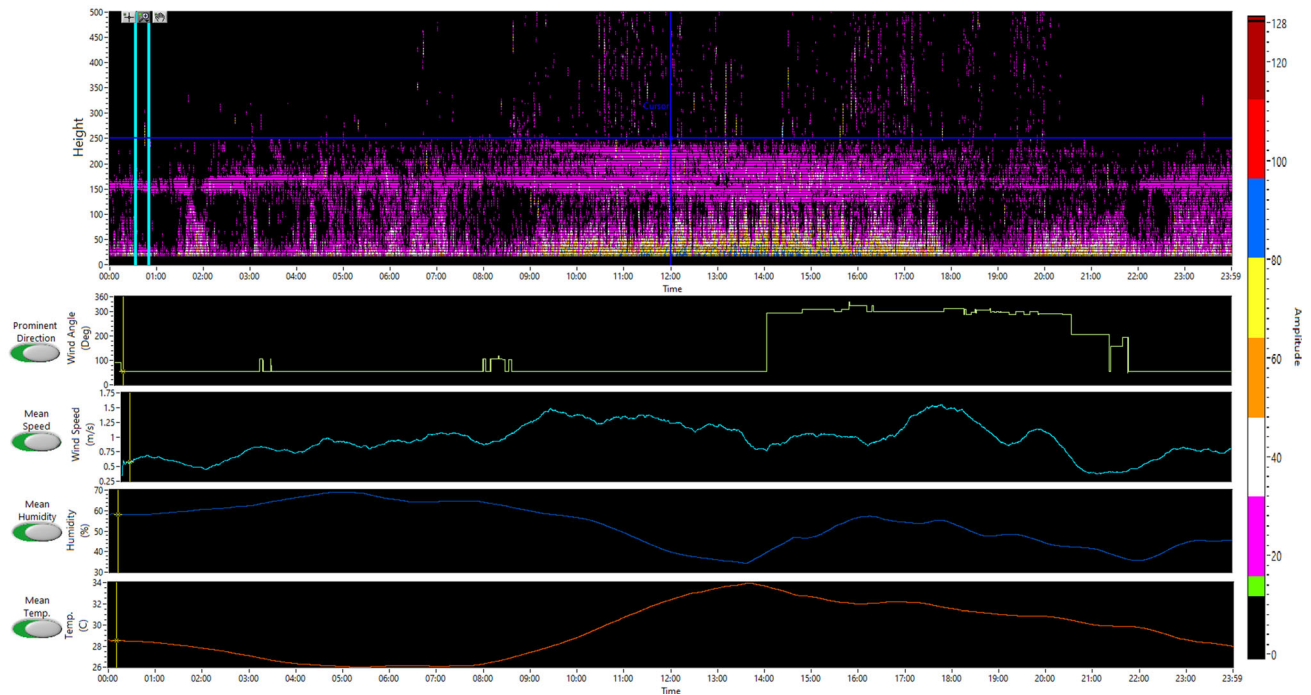


Figure 4. SODAR Echogram (5th November 2020).

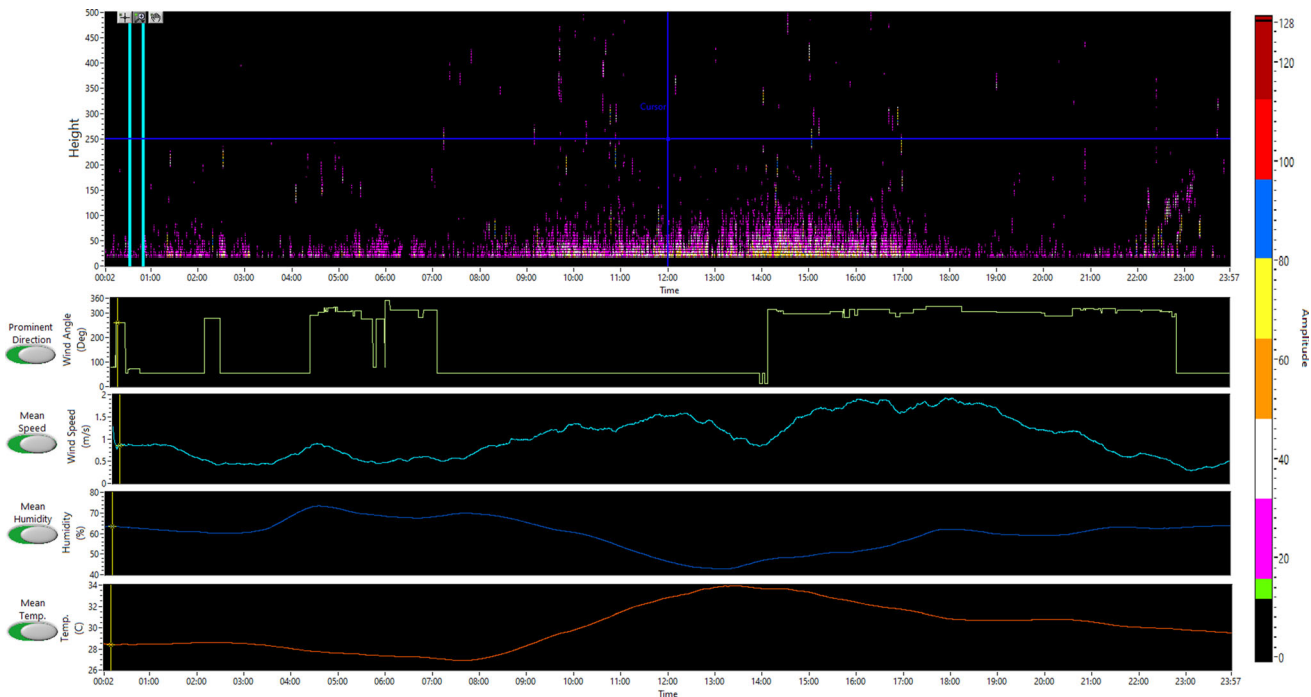


Figure 5. SODAR Echogram (16th November 2020).

The turbulent changes in the ABL due to the development of sea breeze during the daytime and land breeze during night-time give their characteristics signatures on the SODAR echograms. Sea breeze is detected on the SODAR echograms many

times through the formation of capping layer above the daytime slightly diffused thermal plume structure, soon after the erosion of the morning rising inversion layer. Aggarwal *et al.* (1980) studied the atmospheric structure using SODAR

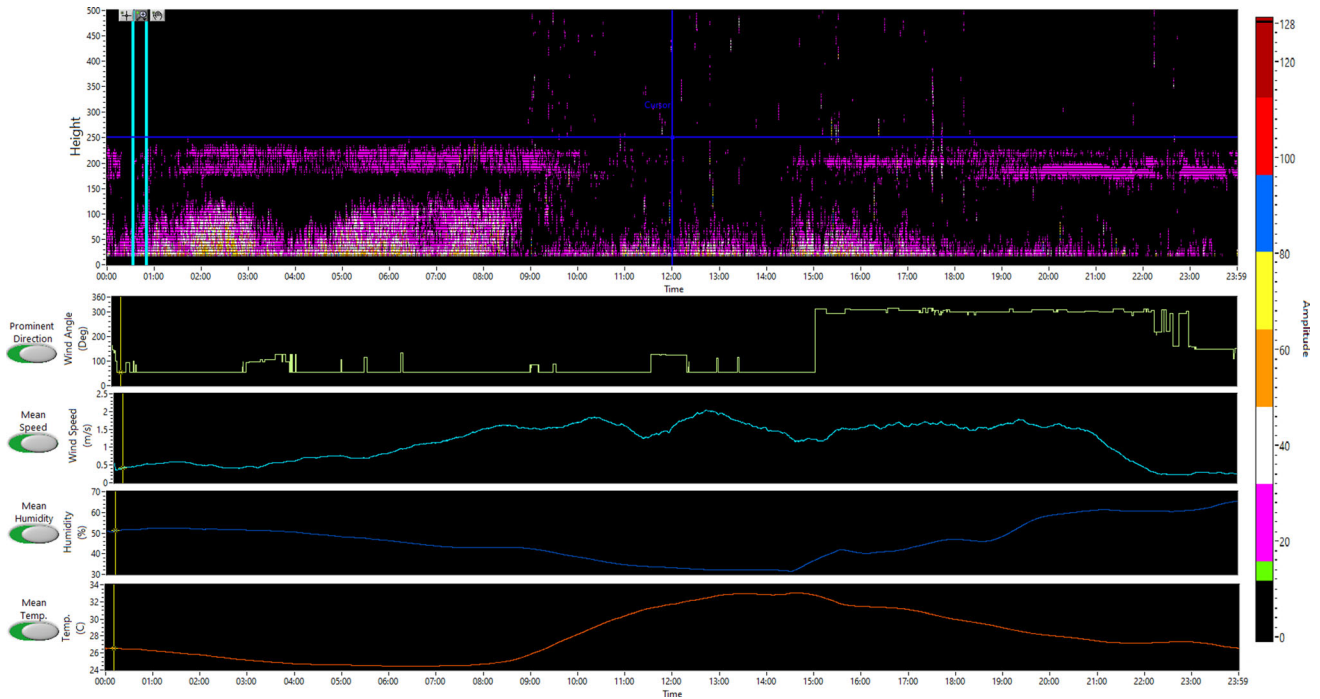


Figure 6. SODAR Echogram (08/12/2020).

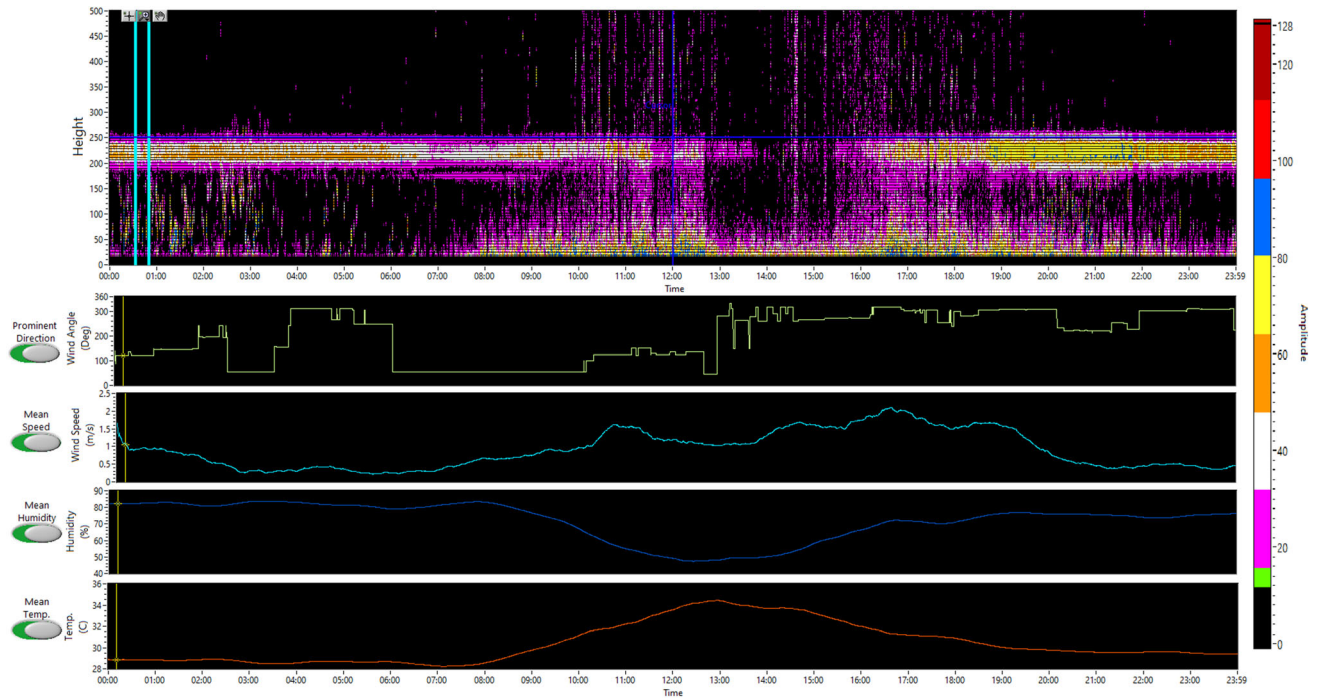


Figure 7. SODAR Echogram (05/04/2021).

and meteorological tower in 1978 at Tarapur and found that thermal convective structures are seen during the daytime and at night time. The height of convective boundary layer in the daytime is 400–500 m, while at night-time, it is mostly under

200 m. Singal (1991) also studied the sea breeze circulation on the Indian coastline (Tarapur and Visakhapatnam) during 1990–1991 and found that continuous real-time data of onset time, duration, and depth of the internal boundary layer during

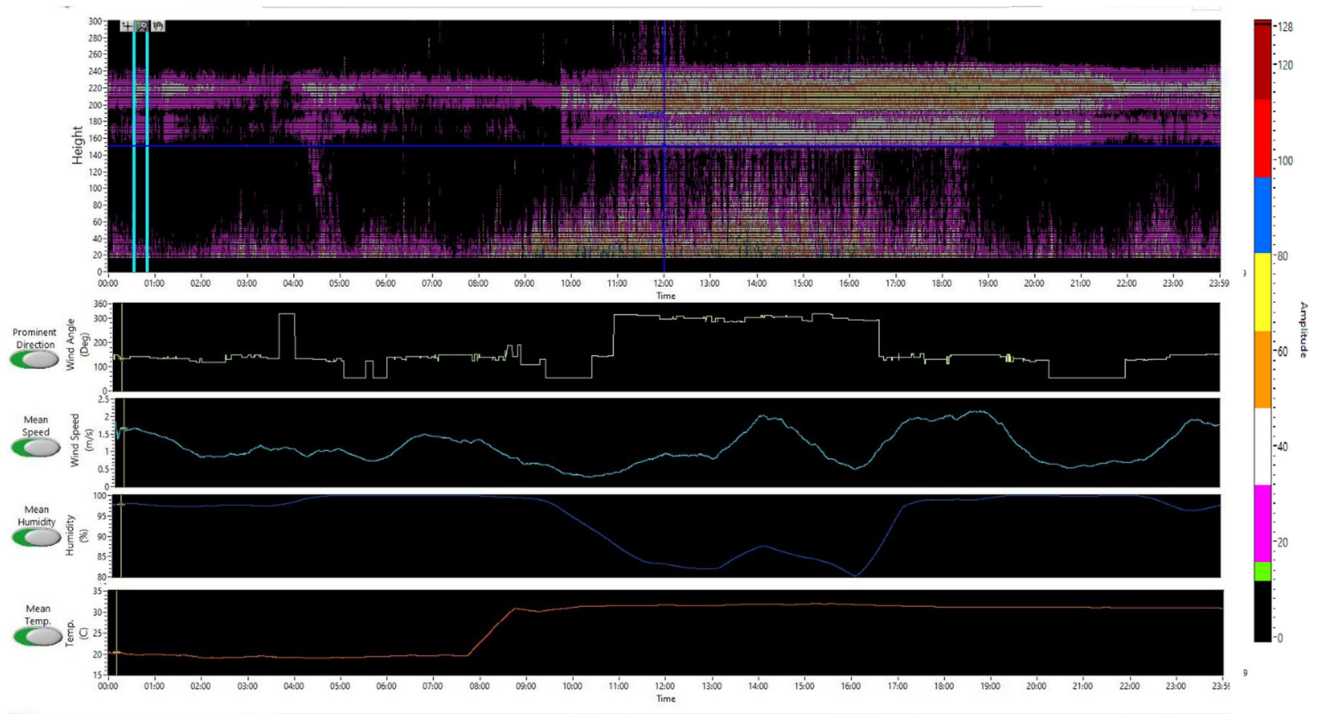


Figure 8. SODAR Echogram (20/09/2021).

Table 2. SODAR data (ABL height with meteorological data) 05/11/2020.

Time	Height (m)	Humidity (%)	Wind speed (m/s)	Wind direction (°)	Temperature (°C)
1:00 AM	80	58.5	0.6	53.5-NE	28.3
2:00 AM	100	60.6	0.5	53.4-NE	27.8
3:00 AM	90	62.4	0.8	54.9-NE	27.1
4:00 AM	90	66.4	0.8	54.6-NE	26.3
5:00 AM	110	68.9	0.9	53.9-NE	26.1
6:00 AM	100	65.7	0.9	53.3-NE	26.1
7:00 AM	110	64.4	1.1	53.7-NE	26.1
8:00 AM	90	64.1	0.9	54.1-NE	26.3
9:00 AM	80	59.8	1.3	53.7-NE	27.4
10:00 AM	570	56.6	1.4	53.6-NE	28.8
11:00 AM	670	49.4	1.3	54.6-NE	30.7
12:00 PM	690	39.9	1.2	53.2-NE	32.4
1:00 PM	610	36	1.2	53.3-NE	33.5
2:00 PM	610	38.9	0.8	54.8-NE	33.7
3:00 PM	640	47	1	308.1-NW	32.6
4:00 PM	570	56.5	0.9	324.1-NW	32
5:00 PM	560	54.4	1.2	300.2-WNW	32.2
6:00 PM	120	54	1.5	312.4-NW	31.5
7:00 PM	100	47.9	0.9	300.5-WNW	31
8:00 PM	80	44.4	1.1	289.0-WNW	30.8
9:00 PM	90	41.6	0.4	204.9-SSW	30
10:00 PM	100	35.7	0.5	54.3-NE	29.8
11:00 PM	80	44.2	0.8	54.9-NE	28.6
12:00 AM	90	45.4	0.8	53.9-NE	28

Table 3. SODAR data (ABL height with meteorological data) 16/11/2020.

Time	Height (m)	Humidity (%)	Wind speed (m/s)	Wind direction (°)	Temperature (°C)
1:00 AM	70	62.1	0.9	54.7-NE	28.5
2:00 AM	70	60.8	0.5	53.7-NE	28.6
3:00 AM	70	60.4	0.4	53.6-NE	28.5
4:00 AM	50	68.6	0.7	54.8-NE	28
5:00 AM	50	72	0.7	305.5-NW	27.6
6:00 AM	80	68.3	0.5	351.1-N	27.3
7:00 AM	80	68.1	0.5	311.5-NW	27.1
8:00 AM	60	69.4	0.8	54.1-NE	27
9:00 AM	70	65.3	1	53.7-NE	28.3
10:00 AM	410	60.5	1.3	54.4-NE	29.8
11:00 AM	430	53.7	1.3	54.7-NE	31.4
12:00 PM	440	46.4	1.5	54.4-NE	32.8
1:00 PM	500	42.9	1.3	53.9-NE	33.8
2:00 PM	500	46.8	0.9	54.8-NE	33.7
3:00 PM	530	49.2	1.6	296.5-WNW	33.3
4:00 PM	490	56.4	1.6	299.2-WNW	31.7
5:00 PM	460	56.3	1.6	299.2-WNW	31.7
6:00 PM	80	62.1	1.9	327.1-NNW	30.8
7:00 PM	60	59.7	1.7	302.3-WNW	30.7
8:00 PM	50	59.1	1.2	300.2-WNW	30.8
9:00 PM	50	61.5	1	318.5-NW	30.6
10:00 PM	50	62.8	0.6	311.0-NW	30
11:00 PM	60	63	0.3	54.4-NE	29.8
12:00 AM	50	63.9	0.5	54.7-NE	29.5

the flow of sea breeze at a coastal site. Gera *et al.* (2013) studied the coastal boundary layer characteristics using the SODAR in the coastal region of the Arabian Sea, Antarctica Ocean and Indian Ocean in 1999, 2001 and 2007, respectively. They found that anomalous thin elevated layers oscillating at periods of about 24 hours in the coastal region.

The phenomena of the sea breeze complexity sparked a lot of interest in understanding the lower troposphere dynamics during sea-breeze events. In coastal areas, the system's sea breeze behaviour and inherent stratification, particularly the Thermal Internal Boundary Layer (TIBL), are critical meteorological elements (Talbot *et al.* 2007). Furthermore, knowing the sea wind is necessary for air quality forecasts and pollution monitoring in highly industrialised and densely populated metropolitan coastal locations (Beyrich *et al.* 1996). During sea breeze situations, TIBL is formed over land with different diffusive characteristics inside and above the TIBL layer (Prabha *et al.* 2002). Prabha *et al.* (2002) also studied the thermal and dynamical influence on the TIBL, which is altered during different synoptic winds,

i.e., changing synoptic conditions from winter to summer pressure patterns over the Indian sub-continent. The onset time and duration of sea breeze are closely associated with the synoptic forcing (Kirankumar *et al.* 2019). Updrafts associated with the sea breeze front are found to be stronger, and turbulence intensity is lower during the weak onshore synoptic wind case (Iwai *et al.* 2011). Reddy *et al.* (2021) studied the characteristics of the sea breeze and TIBL during different seasons at Kattankulathur and Meenambakkam over Chennai and observed that TIBL height is found to be at altitude $\sim 0.54 \pm 0.16$ and 0.62 ± 0.13 km at Meenambakkam and Kattankulathur, respectively. TIBL shows a weak seasonal variation with maximum height during winter and minimum height during summer in contrast to the seasonal variation of the CBL.

In the present study, the ABL height has been estimated using the SODAR echogram as a function of time. Particularly in the months of November, December, January, February, August, September, and October, the ABL height often approached 700 m. The ABL height is increased to 1000–1200 m in April because of the strong wind

Table 4. SODAR data (ABL height with meteorological data) 08/12/2020.

Time	ABL height (m)	Humidity (%)	Wind speed (m/s)	Wind direction (°)	Temperature (°C)
1:00 AM	120	52.3	0.6	53.4-NE	26.3
2:00 AM	140	51.8	0.5	53.7-NE	25.8
3:00 AM	140	51.4	0.4	96.7-E	25.2
4:00 AM	110	50.5	0.7	54.7-NE	24.7
5:00 AM	110	48.2	0.7	54.0-NE	24.6
6:00 AM	140	46.3	0.9	53.5-NE	24.5
7:00 AM	150	43.8	1.2	54.6-NE	24.5
8:00 AM	150	42.8	1.5	54.6-NE	24.7
9:00 AM	120	42.4	1.5	84.8-E	25.8
10:00 AM	400	38.5	1.7	54.7-NE	28.2
11:00 AM	420	34.7	1.6	54.5-NE	30.3
12:00 PM	480	33.2	1.6	125.3-SE	31.7
1:00 PM	530	32.1	1.9	54.5-NE	32.7
2:00 PM	500	32.3	1.5	53.9-NE	32.8
3:00 PM	470	36.5	1.2	53.7-NE	32.8
4:00 PM	590	40.3	1.6	308.3-NW	31.5
5:00 PM	490	42.4	1.6	304.2-NW	31.1
6:00 PM	420	47	1.6	299.3-WNW	30
7:00 PM	70	48.2	1.6	298.3-WNW	29
8:00 PM	70	58.4	1.6	309.3-NW	28.1
9:00 PM	70	61.1	1.3	303.6-NW	27.4
10:00 PM	60	60.6	0.5	299.2-WNW	27.2
11:00 PM	60	61	0.2	158.2-SSE	27.3
12:00 AM	70	65.4	0.3	150.5-SSE	26.6

and temperature. Except for April month, the atmosphere is generally characterised by thermal convection from 0900 to 1800 and thermal inversion from 1900 to 0800. Since there were a large number of ecograms observed throughout the study period, certain ecograms from various seasons are included in this study as it is not possible to represent all ecograms. Figures 4–8 show the structural changes in ABL for the dates of November 5th, 2020 (clear day), November 16th, 2020 (cloudy day), December 8th, 2020 (clear day), April 5th, 2021 (clear day), and September 20th 2021 (cloudy day), respectively. Tables 2–6, on the other hand, include numerical values for ABL height, relative humidity, temperature, wind speed, and wind directions for the same days, respectively.

3.2 Temporal variability of ABL height, ventilation coefficient, and wind speed

Pollutant dispersal capacity and the structure of the lower atmosphere are determined by the ABL

height. The higher the ABL height, the larger the dispersion rate. SODAR echograms show that the ABL height is constantly changing. As a result, the information is conveyed using a box plot. Data values are displayed using a box plot, which shows the level, dispersion, and symmetry of values by plotting data points along the median, quartiles, and lowest and highest points. Every box contains a central mark, which represents the median value, while the bottom line represents the 25th percentile and the top line indicates the 75th percentile of the data. Each outlier is represented by ‘+’ symbol, and the most significant data points are covered by whiskers. An example of temporal ABL height variability is shown in figure 8. The ‘ $\pm\sigma$ ’ standard deviation is shown by the vertical bars. Figure 9 and table 7 show the temporal and monthly ABL height average SODAR data over a period from November 2020 to October 2021. Higher convection period is observed during April (about 1290 m) and the lowest during February (about 330 m). The monthly average maximum value (418 m) of height is measured in April, whereas the lowest value of ABL height (179 m) is found in February month.

Table 5. SODAR data (ABL height with meteorological data) 05/04/2021.

Time	Height (m)	Humidity (%)	Wind speed (m/s)	Wind direction (°)	Temperature (°C)
1:00 AM	110	81.7	1.1	301.3-WNW	28
2:00 AM	130	81	0.8	297.3-WNW	27.9
3:00 AM	120	81.2	0.6	315.2-NW	27.7
4:00 AM	100	81.9	0.8	308.4-NW	27.6
5:00 AM	110	81.3	0.8	306.4-NW	27.5
6:00 AM	100	80.9	0.8	322.2-NW	27.4
7:00 AM	450	80.9	0.7	309.4-NW	27.4
8:00 AM	500	78.2	0.4	53.9-NE	28.1
9:00 AM	610	72.8	0.6	53.6-NE	29.2
10:00 AM	700	69.3	0.9	306.4-NW	29.9
11:00 AM	740	69	1.4	327.3-NNW	30.2
12:00 PM	760	68.4	1.9	301.0-WNW	30.5
1:00 PM	850	67.4	2	321.0-NW	30.7
2:00 PM	830	65.2	2.2	301.5-WNW	31.1
3:00 PM	620	64.3	2.8	305.0-NW	30.9
4:00 PM	520	62.2	3.1	294.5-WNW	30.8
5:00 PM	100	62.6	3.2	307.1-NW	30.7
6:00 PM	90	64.6	2.5	291.2-WNW	30.6
7:00 PM	90	68.7	2.2	299.0-WNW	29.8
8:00 PM	70	70.2	2	309.0-NW	29.4
9:00 PM	60	71.6	1.6	293.6-WNW	29.2
10:00 PM	60	70.1	0.7	300.2-WNW	29.1
11:00 PM	50	64.5	0.7	302.3-WNW	29.1
12:00 AM	50	64.1	0.8	296.5-WNW	29

Figure 10 and table 8 show the temporal and monthly average wind data over a period of nearly a year (November 2020 to October 2021). It is observed that the convection period is most prolonged in April month with a wind speed 7.2 m/s and lowest during December month with a wind speed 1.75 m/s. The monthly average maximum value (4.91 m/s) of wind speed has been observed in July, while the minimum value of wind speed (1.07 m/s) is found during December. Figure 11 shows the monthly wind rose diagram of the above period. It is observed that mostly wind flows in northwest or west direction, but in July month, it flows in only the west direction. The calm wind was absent or less from April to July.

The VC is an atmospheric dispersion value which gives an indication of the air quality and pollution potential, i.e., the capability of the atmosphere to dilute and disperse the pollutants over a location (Sujatha *et al.* 2016). It is calculated as the product of ABL height and the average wind speed. For better atmosphere quality, the value of ventilation coefficient remains

high, i.e., the more efficiently the atmosphere can disperse the pollutants (Kumar *et al.* 2017b). Lower VC values, on the other hand, result in poor pollutant dispersal, stagnation, and poor air quality, potentially resulting in pollution-related problems.

$$VC = ABL \text{ height} \times \text{average wind speed.} \quad (2)$$

The VC is proportional to the height of the ABL and the average wind speed. A change in the VC is caused by variations in the ABL height and average wind speed (Murthy *et al.* 2020). VC less than 6000 m²/s during the afternoon indicates high pollution potential, whereas ABL height of less than 500 m during the morning indicates high pollution potential (Holzworth 1972; Saha *et al.* 2019).

Figure 12 and table 9 show the temporal variation of VC from November 2020 to October 2021. It has been found that overall VC was higher during April (6000–7000 m²/s) due to high ABL height (figure 9) and more change in wind direction (figure 11), and lower during December. During

Table 6. SODAR data (ABL height with meteorological data) 20/09/2021.

Time	Height (m)	Humidity (%)	Wind speed (m/s)	Wind direction (°)	Temperature (°C)
1:00 AM	50	98.5	1.4	153.5-SE	21.3
2:00 AM	50	97.6	1.5	153.4-SE	20.8
3:00 AM	90	97.4	0.8	154.9-SE	20.1
4:00 AM	60	96.4	0.8	344.6-NW	20.3
5:00 AM	70	98.9	0.9	153.9-SE	19.1
6:00 AM	70	99.7	1.2	53.3-NE	20.1
7:00 AM	100	99.4	1.6	53.7-NE	20.1
8:00 AM	300	99.1	0.9	154.1-SE	20.3
9:00 AM	740	99.8	0.8	153.7-SE	27.4
10:00 AM	550	96.6	0.4	53.6-NE	28.8
11:00 AM	570	89.4	0.3	308.1-NW	30.7
12:00 PM	800	85.9	1.2	324.1-NW	31.4
1:00 PM	580	86	1.1	300.2-NW	31.5
2:00 PM	800	88.9	1.8	312.4-NW	30.7
3:00 PM	710	87	1	300.5-NW	32.6
4:00 PM	760	86.5	0.9	289.0-NW	32
5:00 PM	780	94.4	1.2	204.9-SW	32.2
6:00 PM	100	97	1.5	154.3-SE	31.5
7:00 PM	90	97.9	1.9	154.9-SE	31
8:00 PM	50	94.4	1.1	53.9-NE	30.8
9:00 PM	70	98.6	0.7	54.9-NE	30
10:00 PM	50	98.7	0.9	154.3-SE	30.8
11:00 PM	90	94.2	1.5	154.9-SE	30.6
12:00 AM	70	95.4	1.6	153.9-SE	30

November, December, January, February, and September months VC values peak varied from 2000 to 3000 m^2/s (convection period); however, during March, May, July, August, and October, 4000–5000 m^2/s VC values are recorded in convection period. Similarly, in September, VC values between 3000 and 4000 m^2/s are observed during the convection period. Consequently, severe pollution loading conditions occurred from November to February. Sujatha *et al.* (2016) stated that the dispersion of pollutants is dependent upon many meteorological parameters, most significant being wind and ABL height that defines the volume of air through which the pollutant is mixed. As a result, the ventilation coefficient is higher during the daytime and lower at night-time, indicating that the pollution loading capacity of the atmosphere is good during the daytime and poor at night-time.

According to the above results, the ventilation coefficient between daytime and night-time has been significantly different. The ventilation coefficient has been shown in figure 12 and table 9 to tend to be greater and considerably variable during

the daytime, while it was comparatively lower and steady during the night. This might be a consequence of the combined impact of ABL height and wind speed. The existence of ground-based inversions, which impeded the dispersion, may account for the high ABL height values that occur in the afternoon (12:00–14:00), which are mostly attributable to the maximum during the late night and early morning hours (Stull 1988). During pre-monsoon months (April and May) in the afternoon period, high wind speed was observed in comparison to post-monsoon and winter months (September–January). Similar results have also been found for average ABL height, which has been highest during the pre-monsoon months (April and May). These findings showed that daytime ventilation coefficients have been considerably greater than night-time ones, which is favourable for the dispersion of air pollution. While at night, the ventilation coefficient has been seen to be low, which may impede the dispersion of air contaminants and thus lead to poor air quality. It is observed from figures 8 and 9 that afternoons (12:00–14:00 hrs) have very high levels of both

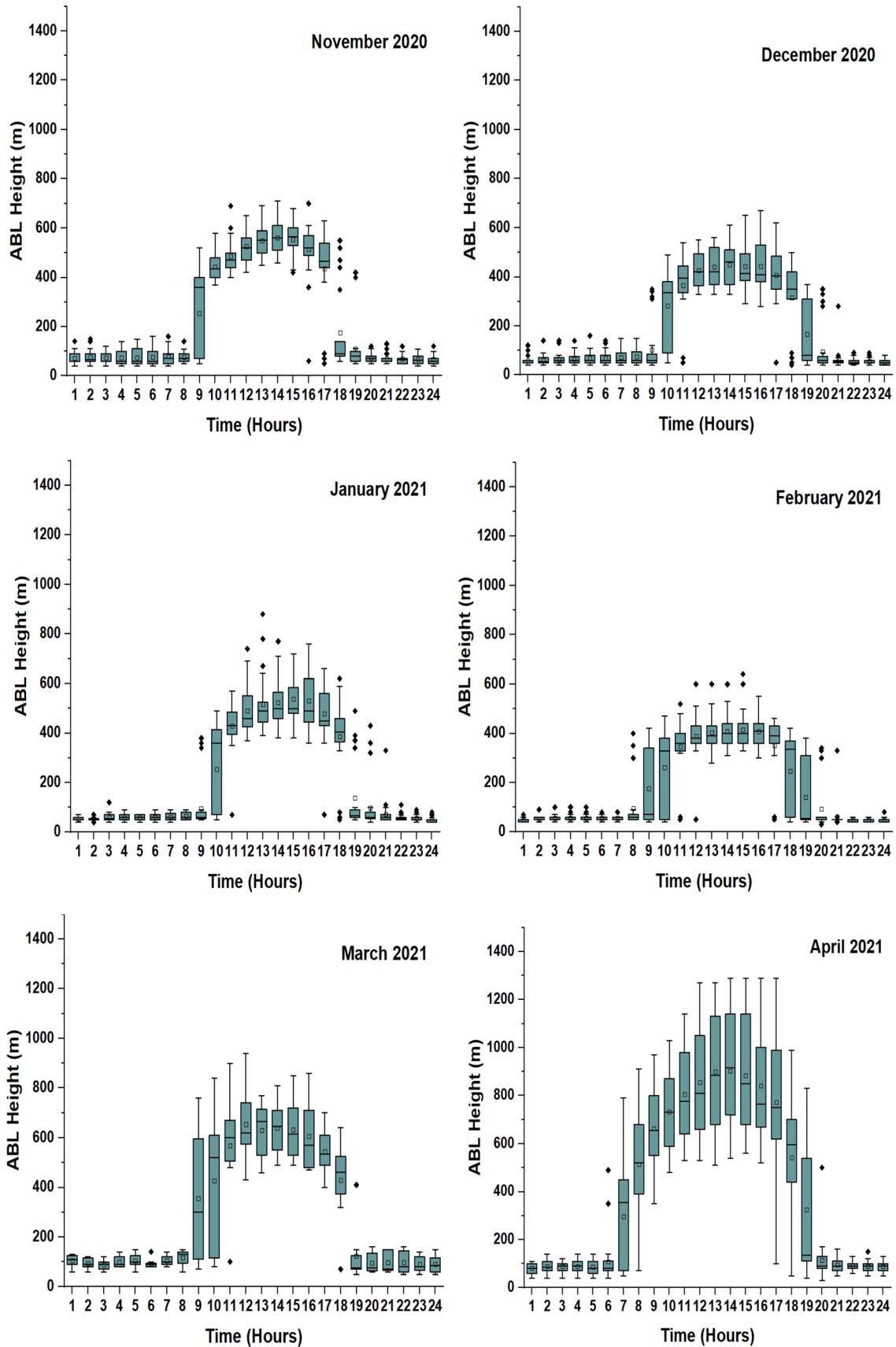


Figure 9. Monthly temporal plot of ABL height.

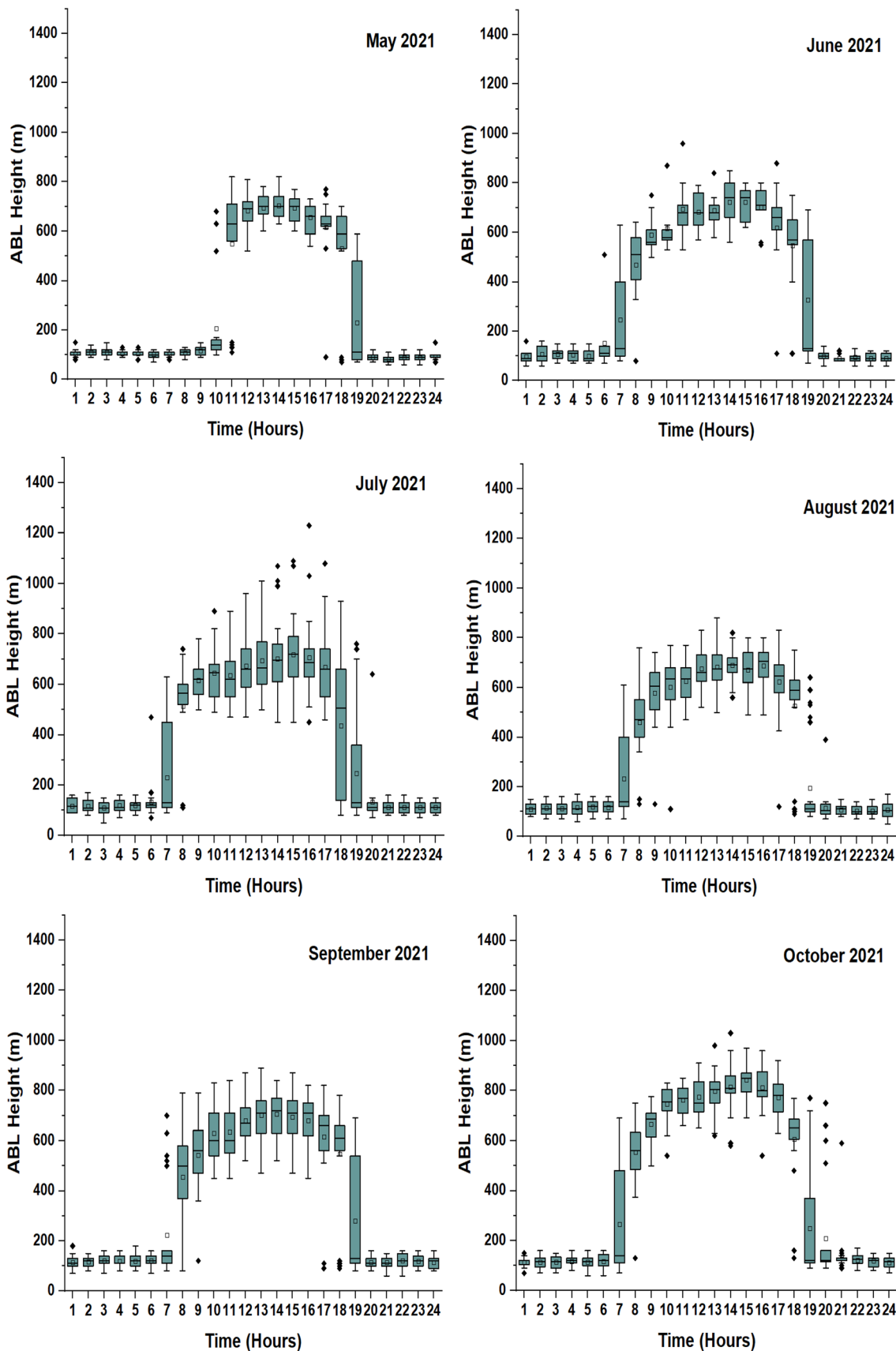


Figure 9. (Continued.)

Table 7. *Monthly ABL height variation during different hours.*

Month	Number of data	Maximum mixing height (m)	Corresponding hour of maximum mixing height (hr)	Average ABL height (m) during		
				Daytime (09:00–18:00 hr)	Remaining hours (19:00–08:00 hr)	Diurnal 24-hr average
November-20	22	710	14:00	449.95	75.58	231.57
December-20	28	670	16:00	368.14	72.81	195.86
January-21	28	880	13:00	424.04	67.02	215.77
February-21	26	640	15:00	340.15	64.95	179.62
March-21	10	940	12:00	549.00	100.27	287.24
April-21	22	1290	14:00	789.67	153.55	418.60
May-21	19	820	14:00	545.00	108.76	290.53
June-21	12	960	11:00	658.67	155.56	365.19
July-21	19	1230	16:00	649.74	163.48	366.09
August-21	18	880	15:00	636.33	151.18	353.33
September-21	24	890	13:00	643.15	161.01	361.90
October-21	27	1030	14:00	759.73	176.15	419.31

Table 8. *Monthly wind speed variation during different hours.*

Month	Number of data	Maximum WS (m.s ⁻¹)	Corresponding hour of maximum WS (hr)	Average WS (m ² .s ⁻¹) during		
				Daytime (09:00–18:00 hr)	Remaining hours (19:00–08:00 hr)	Diurnal 24-hr average
November-20	29	4.87	16:00	2.53	0.90	1.58
December-20	30	4.79	15:00	2.22	0.92	1.46
January-21	31	5.52	17:00	2.65	1.06	1.72
February-21	27	6.03	17:00	2.93	1.16	1.90
March-21	31	6.75	16:00	3.72	1.30	2.31
April-21	28	7.20	16:00	3.92	1.46	2.48
May-21	29	7.23	16:00	3.99	1.77	2.69
June-21	17	5.71	17:00	3.03	1.61	2.20
July-21	30	6.15	14:00	3.77	2.48	3.02
August-21	28	6.09	14:00	3.00	1.73	2.26
September-21	28	5.20	14:00	2.88	1.58	2.12
October-21	31	6.39	16:00	3.08	1.03	1.88

vertical (ABL height) and horizontal (wind speed) ventilation. Nocturnal wind speeds in this study varied from roughly 1–2 m/s, while afternoon wind speeds ranged from 4 to 7.2 m/s, indicating that wind speed in Mumbai is higher during the daytime than at night-time. Krishna *et al.* (2004) also investigated the assimilative capacity of the Visakhapatnam basin region in the pre-monsoon and winter of 2002–2003 using the ventilation coefficient and observed that the ventilation coefficient has the lowest value in the early morning and at night, and has the greatest value in the afternoon.

3.3 *Daily average variability of ABL height, ventilation coefficient, meteorological parameter, and pollutant concentrations*

The ABL structure plays an important role in the formation and evolution of air pollution. The direct measurements of air-pollutant concentrations and SODAR observations have shown that the local contents of pollutants relate to the wind speed and ABL height to a greater extent than with the type of stratification. Wagner and Schafer (2017) proposed that the influence of ABL height on pollutants can be analysed by grouping ABL height data

Table 9. Monthly ventilation coefficient variation during different hours.

Month	Number of data	Maximum VC (m ² /s)	Corresponding hour of maximum VC (hr)	Average VC (m ² /s) during		
				Daytime (09:00–18:00 hr)	Remaining hours (19:00–08:00 hr)	Diurnal 24-hr average
November-20	21	2912	12:00	1211.65	72.67	547.24
December-20	27	2988.20	16:00	860.01	75.35	424.59
January-21	28	3379.20	13:00	1246.81	80.01	566.18
February-21	25	3456	15:00	1060.90	93.13	496.37
March-21	10	4848	16:00	1960.45	115.35	884.14
April-21	22	7095	16:00	3152.79	239.23	1453.21
May-21	19	4598	15:00	2454.74	197.83	1138.21
June-21	19	6071.30	15:00	2450.20	403.13	1256.08
July-21	18	4872	14:00	1958.01	274.20	975.79
August-21	22	3795	16:00	1856.04	250.72	919.60
September-21	24	5242.70	14:00	2456.60	189.37	1134.05

into periods and correlating classified ABL with concentrations of pollutants. To further understand the relation between the ABL height, meteorological parameter, concentration of pollutants and ventilation coefficient, the 24-hourly average value of the concentration of pollutants (PM_{2.5} and PM₁₀), temperature, relative humidity, wind speed, ABL, and ventilation coefficient are presented in figures 13–19. It has been found that ABL, wind speed, temperature, relative humidity, and ventilation coefficient have anti-correlation with the concentrations of pollutants (PM_{2.5} and PM₁₀). Concentrations of pollutants have increased from November 2020 to February 2021 and reached maximum value during January. Variation of ABL has an opposite correlation with the concentrations of pollutants which decrease gradually from March to September. After that, the ABL height and wind speed changed and decreased, and the concentration of pollutants increased from October 2021. The opposite direction indicates that the ABL determine the height of dispersion of the pollutants. Compared to figure 12, it is found that the pollutants have dispersed in the atmosphere during the daytime (08:00–16:00), whereas they accumulated during mid-night-time and early morning time (00:00–08:00).

It is observed from figures 11, 13, 14, 17 and 18, that the southeast winds in Mumbai during November and December 2020 are dominant and as a result, the ABL height is lowest and concentrations of pollutants are greater. However, during January month, the dominance of northwest wind increased, dominance of southeast decreased and

ABL height increased. When the northwest winds are dominant and east/southeast winds are absent or negligible during the March to June 2021 months, then ABL height is increased and the concentration of pollutants is decreased. Again, in September and October months, as southeast winds increased, ABL height decreased and concentration of pollutants also increased. Furthermore, after a sharp drop in temperature (figure 15) throughout these months, a stable and shallow layer developed and persisted at night as a result of substantial surface radiative cooling. Air pollution dispersion is suppressed by stable stratification, calm winds, and humid air conditions (figure 16) in the ABL, which encourages the generation of secondary aerosols. The decrease in northwest winds and increase in southeast winds caused pollutant accumulation in the Mumbai region.

Sengupta (2008) and Nasir and Brahmaiah (2015) have observed that the concentration of the pollutants is not constant throughout the year; its variations indicate that these pollutants are not only affected by the local source, but also remote sources in other locations. From the above result, it has been found that the concentration of pollutants has changed continuously, because of local sources as well as remote sources and meteorological conditions. Simmons *et al.* (1971) and Beran and Hall (1974) found that the concentration of pollutants in any area grows as the square root of the distance along the trajectory when the emission intensity is uniform. Also, the concentration rises parabolically with distance over the source area, and it falls off rapidly at first, then slowly as the air moves further

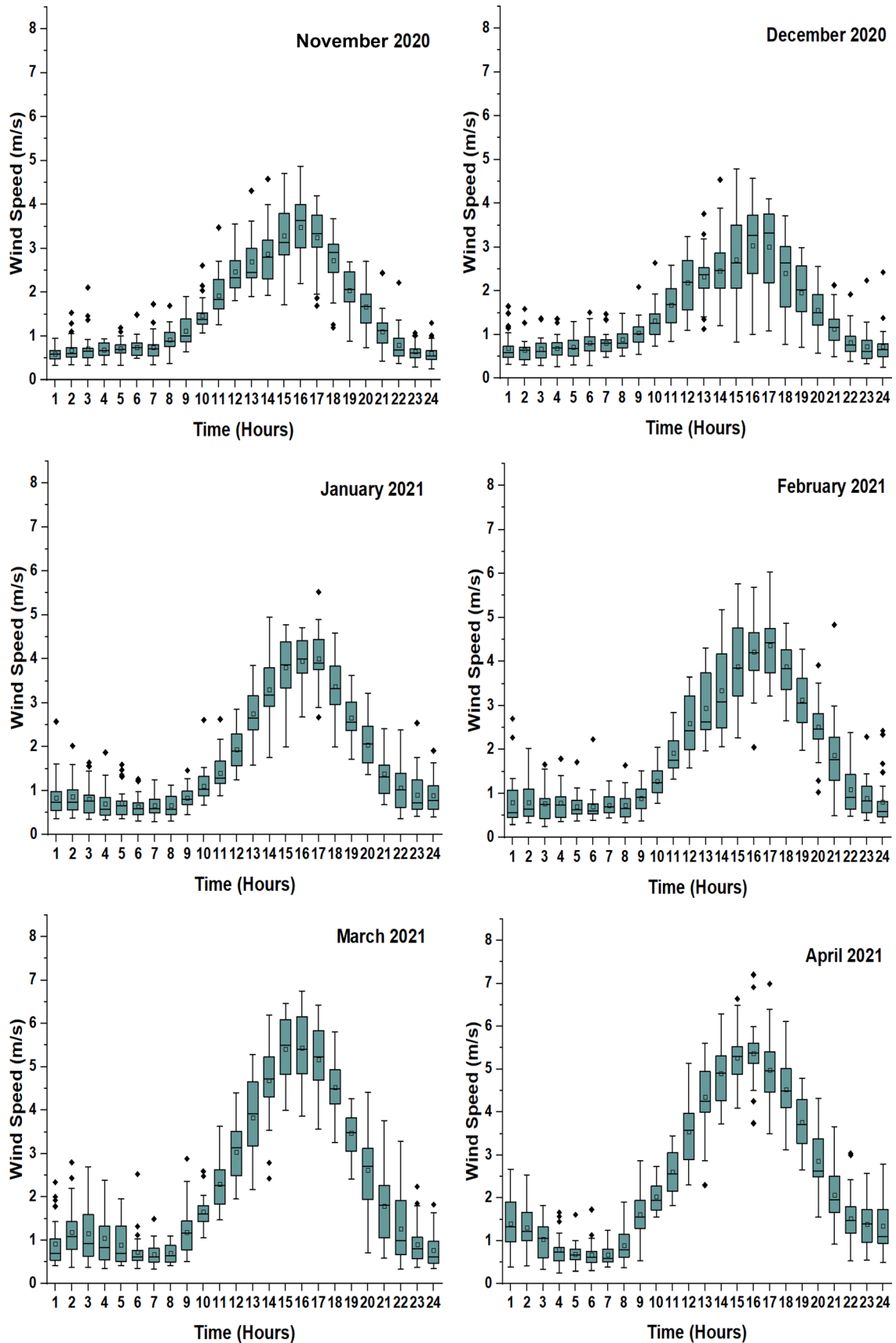


Figure 10. Monthly temporal plot of wind speed.

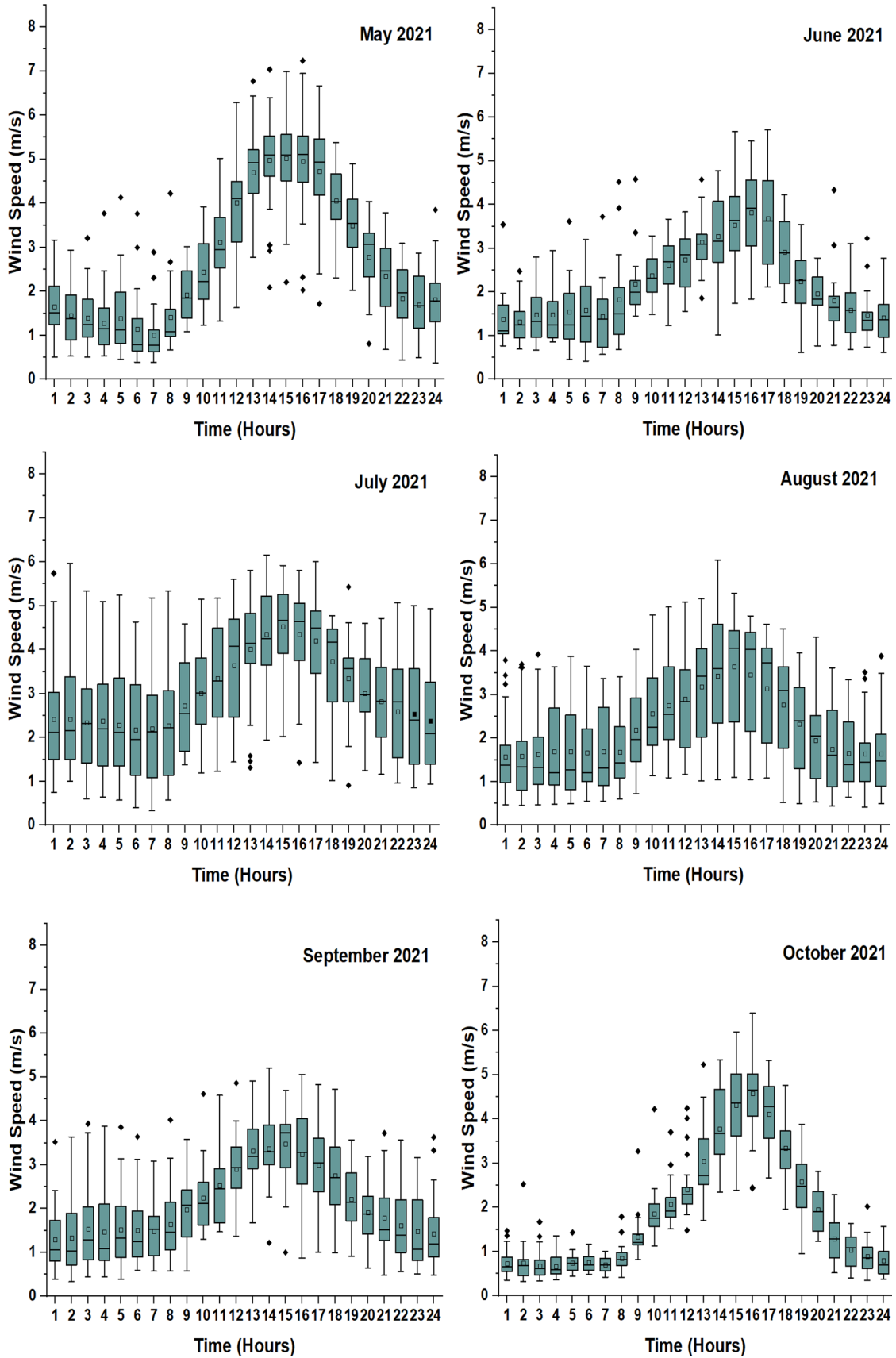


Figure 10. (Continued.)



Figure 11. Monthly wind rose diagram.



Figure 11. (Continued.)

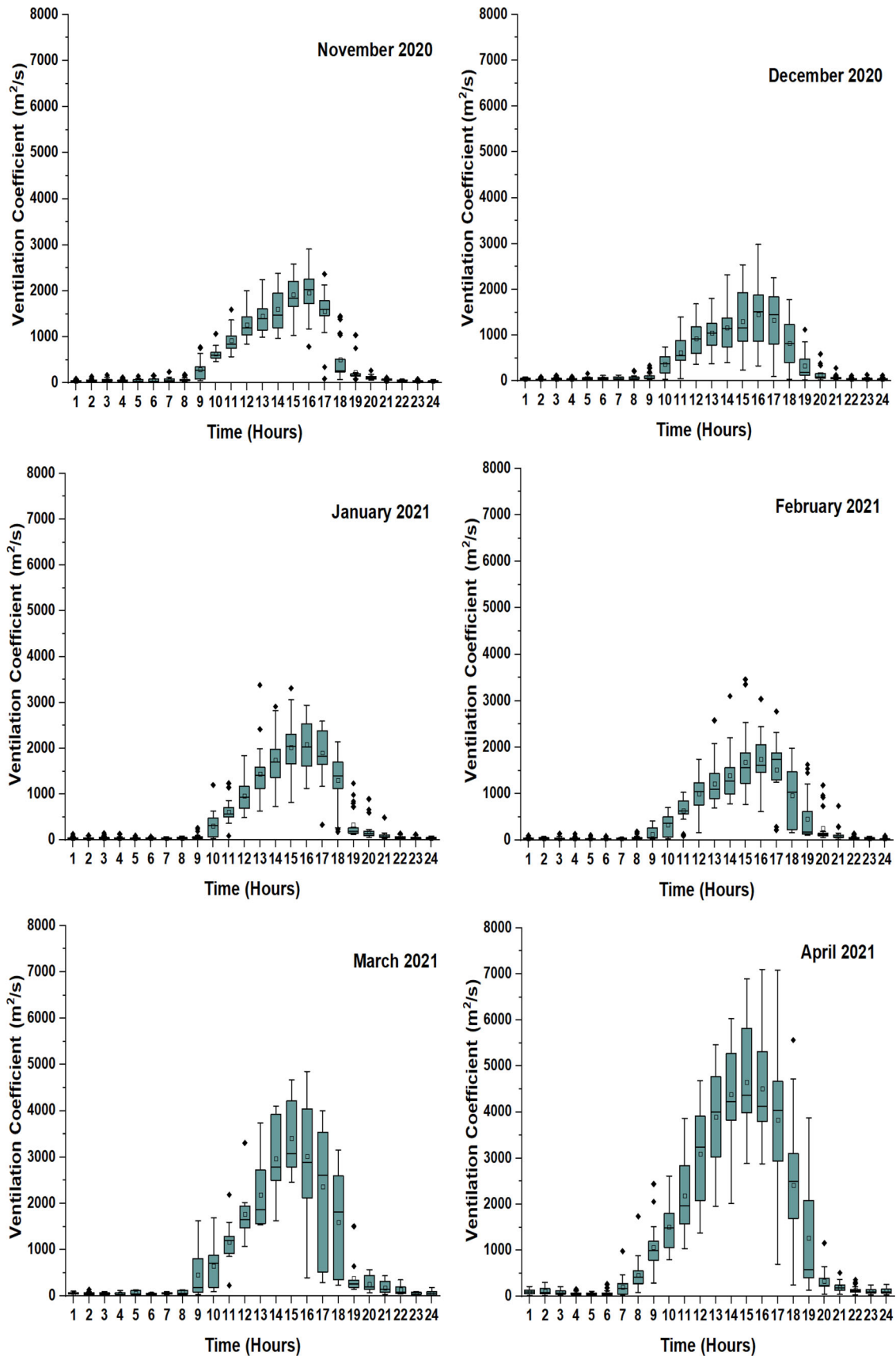


Figure 12. Monthly temporal plot of ventilation coefficient.

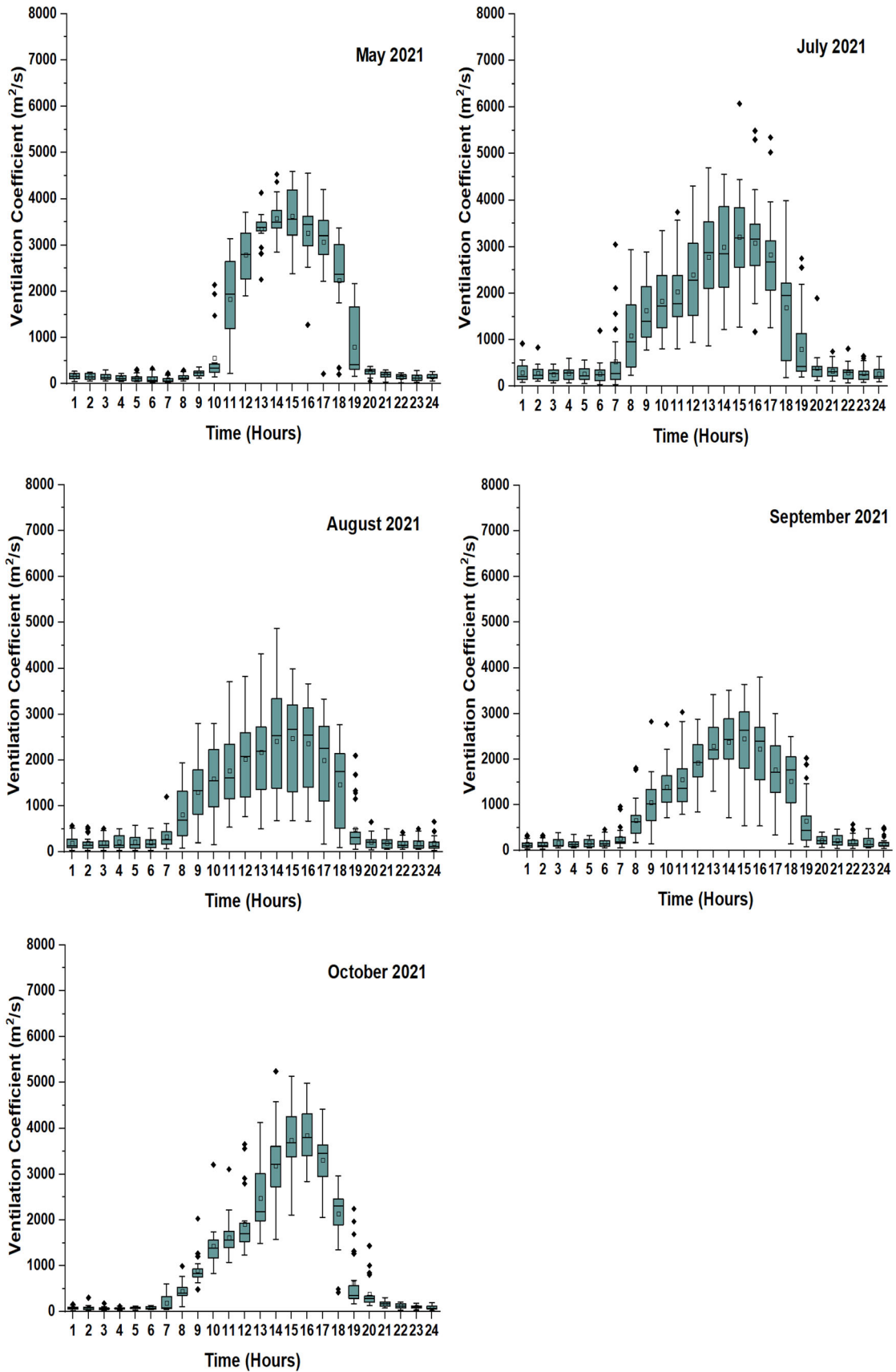


Figure 12. (Continued.)

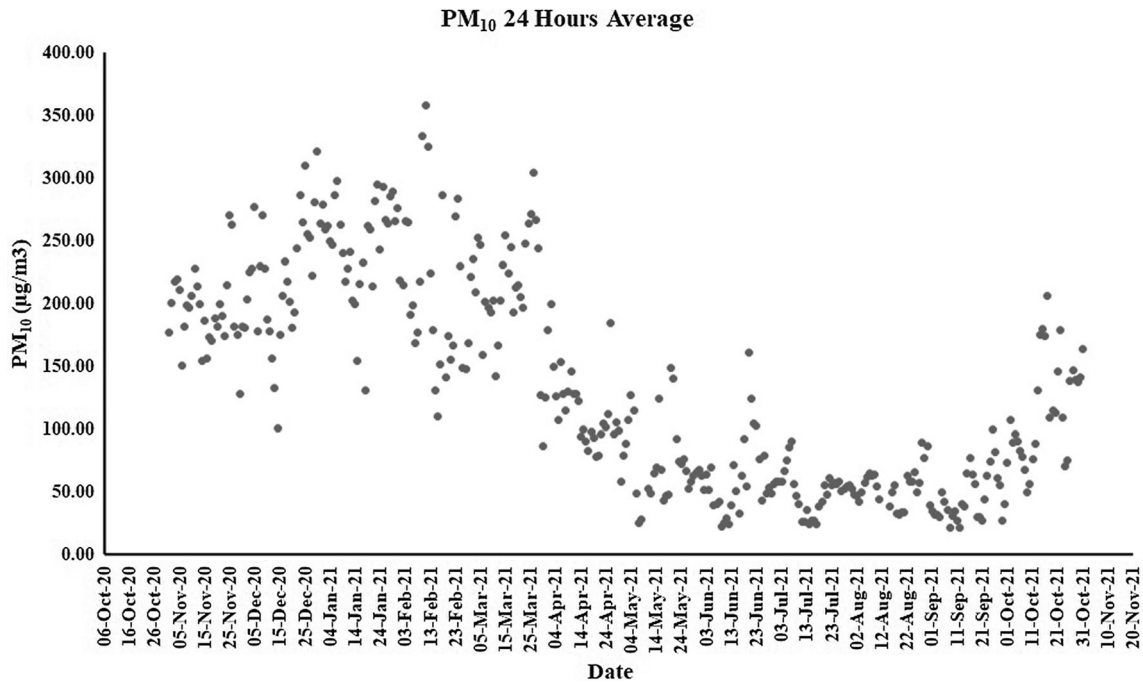


Figure 13. Daily average of PM₁₀.

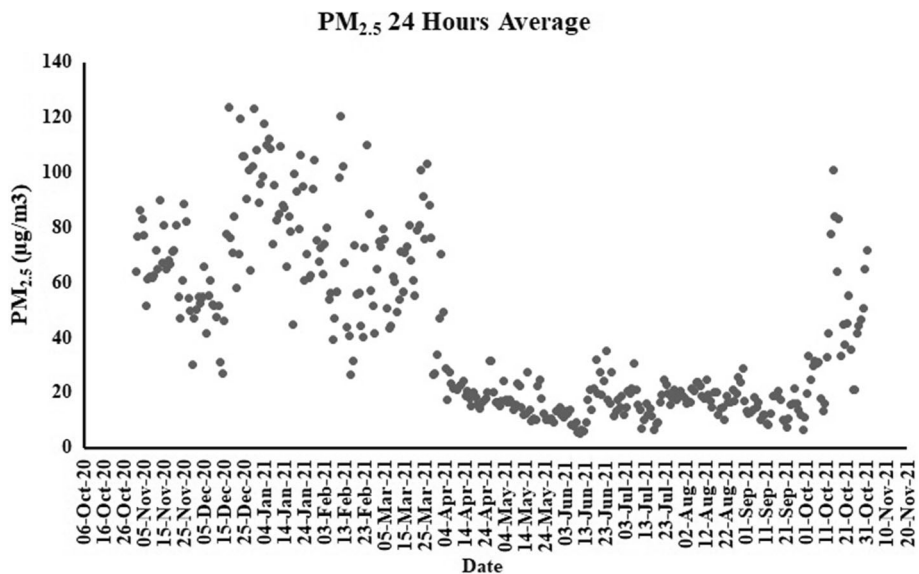


Figure 14. Daily average of PM_{2.5}.

away from the source. Upwind mixing and lateral diffusion can only reduce, not remove, pollutant levels no matter how far downwind they are. Solar heating and winds, to an extent, help to remove pollution, but by far, the most effective process to remove pollutants from the atmospheric air is falling rain. Rain washes away the particles and

gases found in cloud drops and contaminated air. Vittal Murty *et al.* (1980) studied the mixing height and ventilation coefficients for urban centres in India using radiosonde and observed that April recorded the highest values of both maximum and minimum mixing heights for inland and coastal stations. Also, it has been said that higher

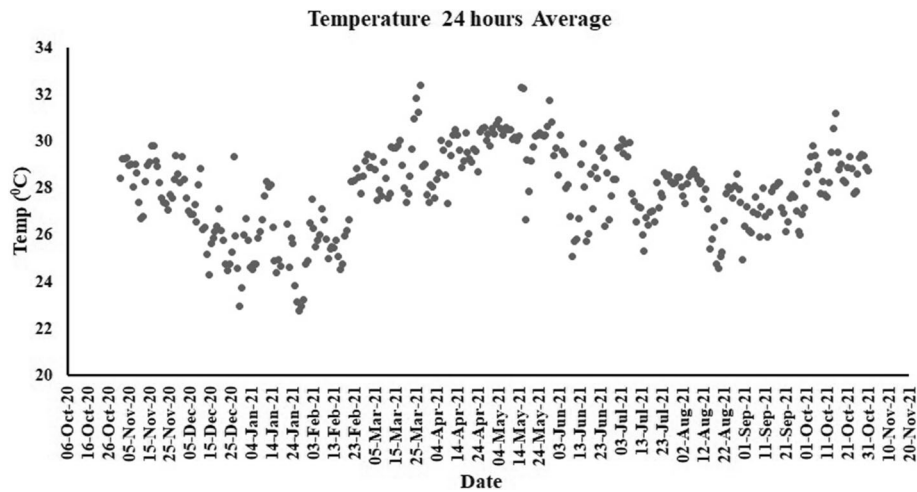


Figure 15. Daily average of temperature.

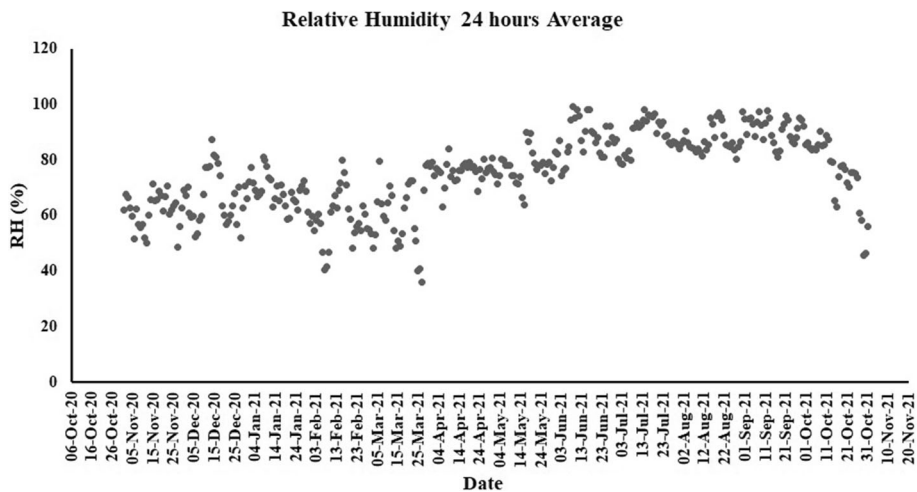


Figure 16. Daily average of relative humidity.

afternoon ventilation coefficients are observed in central India and South India in April and August, respectively.

3.4 Comparison of SODAR and radiosonde measurements

Radiosonde input numerical simulations and assimilation systems are typically used to generate reanalysis datasets. These schemes ensure that the distribution of grid elements is physically and dynamically reasonable. Each reanalysis dataset relies heavily on empirical parameterisations and the diagnostic method chosen, which leads to varying distributions. ERA5 is the fifth generation of ECMWF's (European Centre for Medium-Range Weather Forecasts) global weather and climate

reanalysis product. Compared with the previous version ERA-Interim, this dataset has improved physical drivers and data assimilation methods (Hersbach *et al.* 2020). The greatest advantage of ERA5 is its use of both satellite as well as traditional data for collaborative computation, intercalibration, and processing. It has improved the quality of not only historical observations but also the quality of temporal as well as geographic coverage. ERA5 data has spatiotemporal resolution of $0.25^\circ \times 0.25^\circ$ and 1 h. In this manuscript, the hourly atmospheric boundary layer for a year from November 2020 to October 2021 was extracted over Mumbai.

A comparison of the monthly variation of atmospheric boundary layer height by a SODAR and ERA5 reanalysis data is presented in figure 20

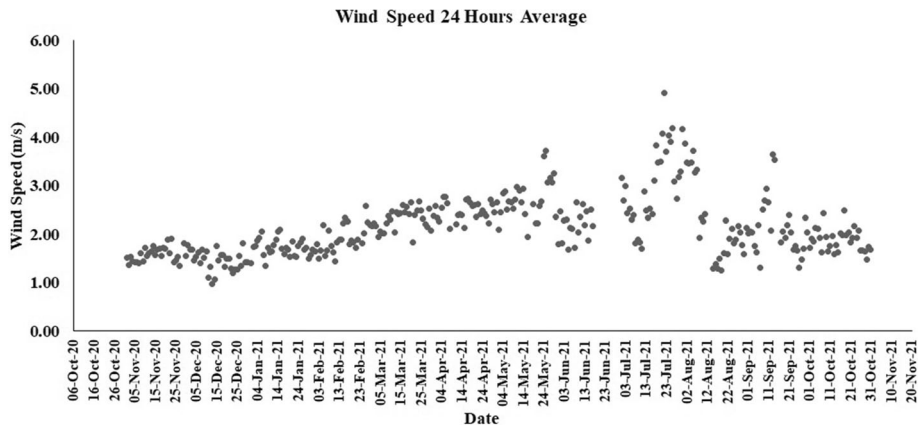


Figure 17. Daily average of wind speed.

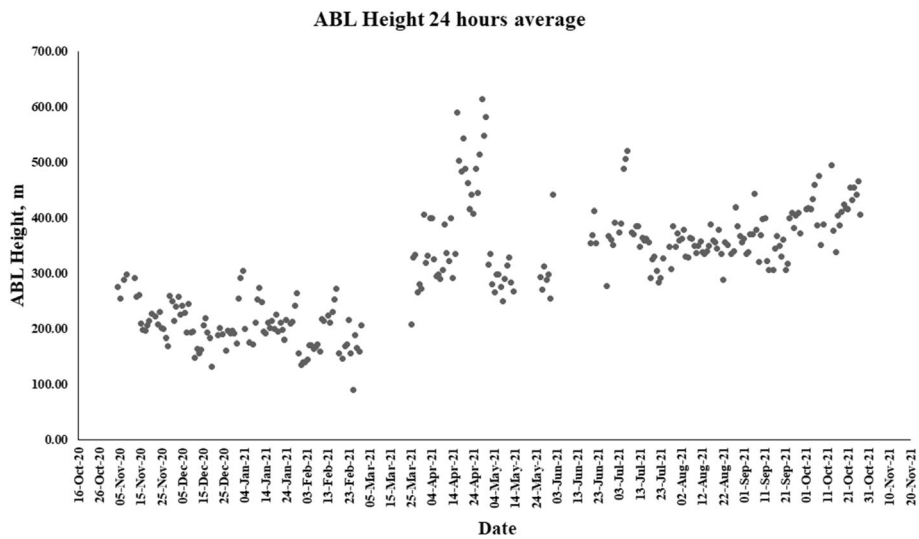


Figure 18. Daily average of ABL height.

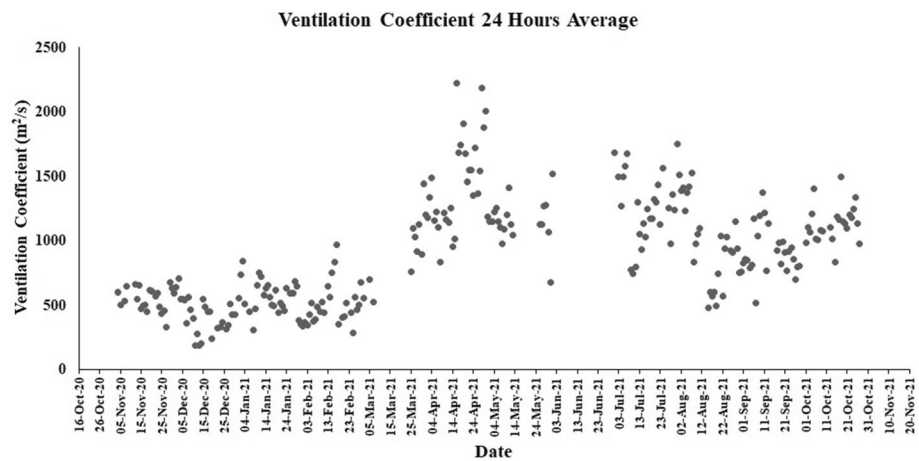


Figure 19. Daily average of ventilation coefficient.

and table 10. It is observed from the figure that the general pattern of variation is similar using both datasets, but the ERA5 reanalysis data values are

higher than the SODAR during all months except October. Each month, diurnal variation of both ERA5 reanalysis data and SODAR dataset is given

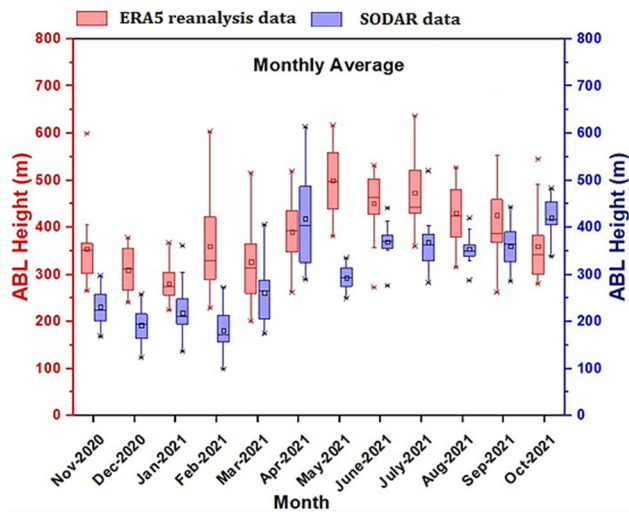


Figure 20. Monthly average variation of ERA5 reanalysis data and SODAR ABL data.

Table 10. Monthly average, max, min values of ERA5 reanalysis data and SODAR data.

Months	ERA5 reanalysis data (m)			SODAR (m)		
	Max	Min	Average	Max	Min	Average
Nov-20	1549	40	354	710	40	231
Dec-20	1251	43	309	670	40	194
Jan-21	1396	40	281	880	40	218
Feb-21	1780	18	359	640	30	180
Mar-21	2063	12	326	940	40	264
Apr-21	1087	23	390	1290	30	418
May-21	1145	31	499	820	60	293
Jun-21	901	98	451	960	60	368
Jul-21	872	154	473	1230	50	366
Aug-21	871	131	430	880	50	353
Sep-21	1001	94	425	890	60	360
Oct-21	1527	24	359	1030	60	420

in the Supplementary file. It is found from both comparisons that Radiosonde ERA5 unstable structure height is higher during November, December, February, and March months, while January, May, June, and July months' height are almost equal. Moreover, during April, SODAR unstable structure height was higher than the ERA5 reanalysis data. On the other hand, stable structure is within 200 m during all the months in SODAR data, however, it varies between 100 and 400 m using ERA5 reanalysis data. During the night-time, surface inversions are caused by the cooling of air upon contact with the cooler ground. Therefore, the SODAR data reveals a deep surface-based layer during the late evening hours that may persist throughout the night unless disturbed by turbulence. This type of structure

implies the presence of a surface-based radiation inversion layer in the lower atmosphere under stable conditions, as depicted in figures containing both SODAR record and ERA5 reanalysis data. The difference can be ascribed to turbulence, which creates a micro-meteorological structure in the lower atmosphere that is unique to a particular location. These observations suggest that turbulence is predominantly of local origin and that more turbulence is generated at and around SODAR sites (Singal and Aggarwal 1979).

4. Conclusion

In the present paper, ABL height variability over Mumbai's coastline area is described using SODAR-based measurements made between November 2020 and October 2021. Due to the existence of the land/sea breeze circulation, the assessment of ABL height over the coastal station is rather complicated. The key findings of the present study are summarised below:

- The ABL height often reached 700 m, especially in November, December, January, February, August, September, and October. Due to the high wind and warmth in April, the ABL height is extended to 1000–1200 m.
- April has the highest convection period (1290 m), while February has the lowest convection time (about 330 m). The highest monthly average height (418 m) is recorded in the month of April, whilst the lowest monthly average height (179 m) is recorded in the month of February.
- It has been noted that the convection period is the longest in the month of April, when the wind speed is 7.2 m/s, and the shortest in the month of December, when the wind speed is 1.75 m/s.
- The monthly average maximum wind speed (4.91 m/s) is recorded in July, while the monthly average lowest wind speed (1.07 m/s) is recorded in December.
- The wind often blows in a northwestern or western direction, however in July, it generally blows in a westward direction. From April through July, the calm breeze is missing or seldom present.
- The highest VC values, around 7095 m²/s are recorded in the month of April, while the lowest values around 2912 m²/s are recorded in the months of November and December.

- It has been observed that the concentrations of pollutants have an anti-correlation with ABL, wind speed, temperature, relative humidity, and ventilation coefficient.
- SODAR dataset is also compared with ERA5 reanalysis dataset, and there is a difference found between the dataset due to the turbulence, which creates a micro-meteorological structure in the lower atmosphere that is unique to a particular location.

Acknowledgements

The authors thank the Director, CSIR-Advanced Materials and Processes Research Institute (AMPRI), Bhopal, for providing the necessary facilities to accomplish the work. The authors are also thankful to the Chairman, Maharashtra Pollution Control Board, Mumbai, for providing funding support.

Author statement

NK and KS are responsible for conceptualisation, data analysis, and writing-original draft. ASN and KAR are responsible for data generation. AAS, AJ and VMM are responsible for proofreading and finalising the draft. VKS and AK are responsible for Radiosonde measurements.

References

- Aggarwal S K, Singal S P, Kapoor R K and Adiga B B 1980 A study of atmospheric structures using sodar in relation to land and sea breezes; *Bound.-Layer Meteorol.* **18**(4) 361–371.
- Beran D W and Hall F F Jr 1974 Remote sensing for air pollution meteorology; *Bull. Am. Meteorol. Soc.* **55**(9) 1097–1106.
- Beyrich F 1997 Mixing height estimation from sodar data – a critical discussion; *Atmos. Environ.* **31**(23) 3941–3953.
- Beyrich F, Acker K, Kala D, Klemm O, Möller D, Schaller E, Werhahn J and Weisensee U 1996 Boundary layer structure and photochemical pollution in the Harz Mountains – An observational study; *Atmos. Environ.* **30**(8) 1271–1281.
- Bontempi E and Coccia M 2021 International trade as critical parameter of COVID-19 spread that outclasses demographic, economic, environmental, and pollution factors; *Environ. Res.* **201** 111514, <https://doi.org/10.1016/j.envres.2021.111514>.
- Bradley S 2007 *Atmospheric Acoustic Remote Sensing: Principles and Applications*; CRC Press, <https://doi.org/10.1201/9781420005288>.
- Brown E H and Hall F F Jr 1978 Advances in atmospheric acoustics; *Rev. Geophys.* **16**(1) 47–110.
- Chourey P, Singh N J, Soni K and Agarwal R 2022a A novel signal conditioning system for SODAR; *Meas. Sci. Technol.* **33**(11) 115801, <https://doi.org/10.1088/1361-6501/ac83e0>.
- Chourey P, Soni K, Singh N J and Agarwal R 2022b IoT-SODAR network for airshed management planning; *IETE J. Res.*, <https://doi.org/10.1080/03772063.2022.2026826>.
- CPCB Report 1992 *National Ambient Air Quality Statistics of India*; <https://cpcb.nic.in/>.
- EPA Report 2000 *Meteorological Monitoring Guidance for Regulatory Modeling Applications*, EPA; https://www.epa.gov/sites/production/files/2020-10/documents/mmgrma_0.pdf.
- Garratt J R 1994 The atmospheric boundary layers; *Earth Sci. Rev.* **37**(1–2) 89–134.
- Gera B S, Raghavendra T, Singh G, Ojha V K, Malik J, Gera N and Gupta N C 2011 Instrumentation and computer capabilities for improving sodar data acquisition; *Int. J. Remote Sens.* **32**(17) 4807–4817.
- Gera B S, Gera N, Gupta N C, Malik J, Singh G and Ojha V K 2013 Sodar studies of coastal boundary layer characteristics; <https://www.ursi.org/proceedings/procGA08/papers/F02p5.pdf>.
- Hersbach H, Bell B and Berrisford P *et al.* 2020 The ERA5 global reanalysis; *Quart. J. Roy. Meteorol. Soc.* **146** 1999–2049, <https://doi.org/10.1002/qj.3803>.
- Holzworth G C 1972 *Mixing heights, wind speeds, and potential for urban air pollution throughout the contiguous United States*; US Government Printing Office.
- Iwai H, Murayama Y, Ishii S, Mizutani K, Ohno Y and Hashiguchi T 2011 Strong updraft at a sea-breeze front and associated vertical transport of near-surface dense aerosol observed by Doppler lidar and ceilometer; *Layer Meteorol.* **141** 117–142.
- Kallistratova M A 1963 *Experimental investigation of sound wave scattering in the atmosphere*; Foreign Technology Division, Wright-Patterson, AFB, OHIO.
- KiranKumar N V P, Jagadeesh K, Niranjana K and Rajeev K 2019 Seasonal variations of sea breeze and its effect on the spectral behaviour of surface layer winds in the coastal zone near Visakhapatnam, India; *J. Atmos. Sol.-Terr. Phys.* **186** 1–7.
- Krishna T R, Reddy M K, Reddy R C and Singh R N 2004 Assimilative capacity and dispersion of pollutants due to industrial sources in Visakhapatnam bowl area; *Atmos. Environ.* **38**(39) 6775–6787.
- Kumar N K, Rao C K, Sandeep A and Rao T N 2014 SODAR observations of inertia-gravity waves in the atmospheric boundary layer during the passage of tropical cyclone; *Atmos. Sci. Lett.* **15**(2) 120–126.
- Kumar A, Gupta I, Brandt J, Kumar R, Dikshit A K and Patil R S 2016 Air quality mapping using GIS and economic evaluation of health impact for Mumbai city, India; *J. Air Waste Manag.* **66**(5) 470–481.
- Kumar N, Soni K, Garg N, Agarwal R, Saha D, Singh M and Singh G 2017a SODAR pattern classification and its dependence on meteorological parameters over a semi-arid region of India; *Int. J. Remote Sens.* **38**(11) 3466–3482.
- Kumar N, Soni K, Agarwal R and Singh M 2017b SODAR as a diagnostics tool for urban air-quality and health care system; *J. Acoust. Soc. India* **44** 213–222.

- Kumar N, Soni K and Agarwal R 2021a A comprehensive study of different feature selection methods and machine-learning techniques for SODAR structure classification; *Model. Earth Syst. Environ.* **7(1)** 209–220.
- Kumar N, Soni K and Agarwal R 2021b Design and development of SODAR Antenna structure; *MAPAN-J. Metrol. Soc. I.* **36(4)** 785–793.
- Kumar N, Soni K and Agarwal R 2021c Prediction of temporal atmospheric boundary layer height using long short-term memory network; *Tellus a: Dyn. Meteorol. Oceanogr.* **73(1)** 1–14.
- Liao L, Du M and Chen Z 2021 Air pollution, health care use and medical costs: Evidence from China; *Energy Econ.* **95** 105132, <https://doi.org/10.1016/j.eneco.2021.105132>.
- Murthy B S, Latha R, Tiwari A, Rathod A, Singh S and Beig G 2020 Impact of mixing layer height on air quality in winter; *J. Atmos. Sol.-Terr. Phys.* **197** 105157, <https://doi.org/10.1016/j.jastp.2019.105157>.
- Nasir U P and Brahmaiah D 2015 Impact of fireworks on ambient air quality: A case study; *Int. J. Environ. Sci. Technol.* **12(4)** 1379–1386.
- Prabha T V, Venkatesan R, Mursch-Radlgruber E, Rengarajan G and Jayanthi N 2002 Thermal internal boundary layer characteristics at a tropical coastal site as observed by a mini-SODAR under varying synoptic conditions; *J. Earth Syst. Sci.* **111(1)** 63–77.
- Reddy T V, Mehta S K, Ananthavel A, Ali S, Annamalai V and Rao D N 2021 Seasonal characteristics of sea breeze and thermal internal boundary layer over Indian east coast region; *Meteorol. Atmos. Phys.* **133(2)** 217–232.
- Saha D, Soni K, Mohanan M N and Singh M 2019 Long-term trend of ventilation coefficient over Delhi and its potential impacts on air quality; *Remote Sens. Appl.: Soc. Environ.* **15** 100234, <https://doi.org/10.1016/j.rsase.2019.05.003>.
- Seibert P, Beyrich F, Gryning S E, Joffre S, Rasmussen A and Tercier P 2000 Review and intercomparison of operational methods for the determination of the mixing height; *Atmos. Environ.* **34(7)** 1001–1027.
- Sengupta B 2008 Epidemiological study on effect of air pollution on human health (adults) in Delhi; https://cpcb.nic.in/uploads/healthreports/Epidemiological_study_Adult_Peer%20reviewed-2012.pdf.
- Simmons W R, Wescott J W and Hall F F 1971 *Acoustic echo sounding as related to air pollution in urban environments*; Vol. 2, Environmental Research Laboratories.
- Singal S P 1991 SODAR studies of sea breeze circulation of Indian coastline; *Indian J. Radio Space Phys.* **20** 397–401.
- Singal S P 1993 Monitoring air pollution related meteorology using sodar; *Appl. Phys. B Photophys. Laser Chem.* **57(1)** 65–82.
- Singal S P and Aggarwal S K 1979 Sodar & radiosonde studies of thermal structure of the lower atmosphere at Delhi; *Indian J. Radio Space Phys.* **8** 76–81.
- Singal S P, Aggarwal S K, Pahwa D R and Gera B S 1985 Stability studies with the help of acoustic sounding; *Atmos. Environ.* **19(2)** 221–228.
- Singal S P, Gera B S and Pahwa D R 1994 Application of sodar to air pollution meteorology; *Remote Sens.* **15(2)** 427–441.
- Singal S P, Gera B S and Saxena N 1997 Sodar: A tool to characterise hazardous situations in air pollution and communication; In: *Acoustic Remote Sens. Appl.* (ed.) Sagar Pal Singal, pp. 325–384.
- Stull R B 1988 *An introduction to boundary layer meteorology*; Vol. 13, Springer Science & Business Media, <https://doi.org/10.1007/978-94-009-3027-8>.
- Sujatha P, Mahalakshmi D V, Ramiz A, Rao P V N and Naidu C V 2016 Ventilation coefficient and boundary layer height impact on urban air quality; *Cogent Environ. Sci.* **2(1)** 1125284, <https://doi.org/10.1080/23311843.2015.1125284>.
- Talbot C, Augustin P, Leroy C, Willart V, Delbarre H and Khomenko G 2007 Impact of a sea breeze on the boundary-layer dynamics and the atmospheric stratification in a coastal area of the North Sea; *Bound.-Layer Meteorol.* **125(1)** 133–154.
- Vittal Murty K P R, Viswanadham D V and Sadharam Y 1980 Mixing heights and ventilation coefficients for urban centres in India; *Bound.-Layer Meteorol.* **19(4)** 441–451.
- Wagner P and Schäfer K 2017 Influence of mixing layer height on air pollutant concentrations in an urban street canyon; *Urban Clim.* **22** 64–79.